Interleave Division Multiple Access for Broadband Wireless Communications

Kun Wu

A thesis submitted to
School of Information Science,
Japan Advanced Institute of Science and Technology,
in partial fulfillment of the requirements
for the degree of
Master of Information Science
Graduate Program in Information Science

Written under the direction of
Professor Tadashi Matsumoto

September, 2014

Interleave Division Multiple Access for Broadband Wireless Communications

Kun Wu (1210204)

A thesis submitted to
School of Information Science,
Japan Advanced Institute of Science and Technology,
in partial fulfillment of the requirements
for the degree of
Master of Information Science
Graduate Program in Information Science

Written under the direction of
Professor Tadashi Matsumoto

and approved by
Professor Tadashi Matsumoto
Associate Professor Brian Michael Kurkoski
Associate Professor Kiyofumi Tanaka

August, 2014 (Submitted)

I certify that I have prepared this Master's Thesis by myself without any inadmissible outside help.

Kun Wu
JAIST, Aug. 7, 2014

Author : _____

Date : _____

Supervisor : _____

Acknowledgments

First and foremost, I would like to express my sincerest gratitude to my supervisor, Professor Tadashi Matsumoto, who gives me the continuous support and encouragement of my study and research. I am grateful for his guidance, care, patience, and providing me with an excellent and international atmosphere for doing research. I learned a lot from him not only academic knowledge but also the life experiences which will deeply benifit me through my life.

Besides my supervisor, I am grateful for my co-supervisor Associate Professor Brian Michael Kurkoski for his valuable help and comments of my study and research. My sincere thanks also goes to Assistant Professor Khoirul Anwar for his patient guidance and helpful advices. I would like to thank Associate Professor Kiyofumi Tanaka for his valuable comments and suggestions, and Associate Professor Shinobu Hasegawa for his careful guidance of my minor research.

I would like to devote my sincere thanks to all my colleagues in our laboratory for their selfless help and precious friendship. This thesis is also in memory of one of the most excellent and honorable graduates from this laboratory, Kisho Fukawa, who passed away last October. His research work on (EXIT)-constrained Binary Switching Algorithm (EBSA) greatly inspired me and played an important role in my research.

Furthermore, I would like to thank all the staff in this university who provide me a lot of help and convenience of my studying and living here. I would also like to thank my friends for their kind care and help.

Last but not the least, I would like to express my sincere gratitude to my parents and my sister for their love, support and encouragement. I would also like to give my sincere gratitude to my fiancee, without her endless love and support, I could not have completed this work.

Abstract

This thesis investigates an up-link multiple access technique with interleave division multiple access (IDMA) of which the crucial requirement is the proper operability at a very low signal-to-interference-plus-noise power ratio (SINR) value range. The primary objectives of this thesis are twofold: (1) to design and evaluate IDMA systems based on bit interleaved coded modulation with iterative detection (BICM-ID) and optimization of the BICM-ID system using extrinsic information transfer (EXIT)-constrained Binary Switching Algorithm (EBSA) over additive white Gaussian noise (AWGN) channels, (2) to further jointly utilize a frequency domain soft-interference cancelation minimum mean-square error (FD-SC-MMSE) turbo equalization in frequency selective fading channels. Particularly, in order to further improve the performance of the system and verify the superiority of the proposed system, the impact of the power allocation on the convergence and the multiple access channel (MAC) rate region, robustness against the asynchronism and the impact of detection ordering are also investigated.

First of all, this thesis focuses on the IDMA system design that requires proper operability at a very low SINR range in AWGN channels. The achievability of near-capacity performance of BICM-ID, using very low rate single parity check and irregular repetition (SPC-IrR) codes at a very low SINR range, is demonstrated. The technique is hence effective in achieving excellent performance when it is applied for IDMA; then, a very simple multiuser detection (MUD) technique for the SPC-IrR BICM-ID IDMA is proposed, which does not require heavy per-iteration computational burden; after that, the impacts of power allocation on the convergence property of MUD as well as on the rate region is analyzed by using EXIT chart; moreover, performance sensitivity to frame-asynchronism of the proposed system is investigated. The SPC-IrR code parameters and the modulation labeling patterns are optimized by using the EBSA technique at a very low SINR range. Simulation results show that the proposed technique can achieve excellent near-capacity performance with the bit error rate (BER) curves exhibiting very sharp threshold, which significantly influences the convergence property of MUD. Then, this thesis presents results of the multiple access rate region analysis in the cases of equal and unequal power allocation. The results of the rate region analysis for a counterpart technique is also presented. The results of the MAC rate region analysis show that our proposed technique outperforms the counterpart technique. Furthermore, the results of series simulations indicates the robustness of the proposed IDMA technique against frame-asynchronism.

This thesis then aims to combine turbo equalization and BICM-ID-based IDMA techniques over frequency selective fading channels. The codes parameters and modulation labeling patterns are also optimized by EBSA at a very low SNR range. FD-SC-MMSE turbo equalization is used together with IDMA signal detection to detect all the simultaneous users. Moreover, a detection ordering (DO) technique is proposed to improve the efficiency of the detection scheme. Simulation results show that the proposed technique can eliminate the influences of both intersymbol interference (ISI) and multiple access interference (MAI), due to, respectively, the fading frequency selectivity and the channel sharing with other simultaneous users, and achieve the excellent frame error rate (FER) performance in the cases of single, 8 and 10 simultaneous users although the user number is larger than its equivalent spreading factor. The comparison of the performances between the system with and without DO shows that significant performance improvement with DO technique can be achieved.

Keywords: IDMA, BICM-ID, EBSA, single user detection (SUD), MUD, turbo equalization, power allocation, asynchronism, detection ordering, BER, FER, MAC rate region, EXIT chart, Shannon limit, outage probability, AWGN, frequency selective fading

Contents

List of Figures

Chapter 1

Introduction

1.1 Background and Motivation

In modern wireless communications, Code Division Multiple Access (CDMA) and its family technologies are widely used as technical standards. However, with the rapid growth of users, the system user capacity of CDMA is now being approached due to multiple access interference (MAI) as well as inter-symbol interference (ISI). With the invention of turbo codes [1], the significant progress on mitigating MAI and ISI by iterative multiuser-detection (MUD) has been made. Since the achievability of the multiple access channel (MAC) capacity region has been theoretically proven in [2, 3], many researches have tried to design the practical systems that can achieve the performance as close to the capacity region as possible. The superiority of CDMA systems with the entire bandwidth-expansion factor being allocated only for error correction coding by using very low rate code, where no spreading is used, is well known as a fundamental concept of communication theory [4]. To make effective use of this theoretical background, a CDMA technique with chip-level interleaving is proposed in [5] (in fact, [5] presents the original idea of interleave division multiple access (IDMA)). The IDMA concept was reformulated and introduced in [6, 7] and [8].

IDMA actually can be seen as a transmission technique derived on the basis of CDMA but it has a variety of design flexibility and exhibits performance superiority, in general. In CDMA, channel coding for error protection and spreading for user separation are performed independently, while in IDMA, random interleaving is included in the iteratively decodable channel code, and is also used for user separation. Therefore, the total bandwidth can be, fully and directly, allocated for the channel coding only. IDMA also inherits many advantages from CDMA, such as that it can achieve path diversity gain to cope

with fading channel variation, and that it can reduce the influence of interference having large received signal energy.

It is well known that the smaller the rate of the code used, the lower the signal-to-interference-plus-noise power ratio (SINR) required to achieve arbitrarily low message error rate. In this sense, IDMA has a higher potential for accommodating large number of users than CDMA techniques that encodes the information sequence by a channel code first, and then spreads the coded sequence bit-by-bit. This is because spreading is equivalent to repetition coding, which only achieves a gain in signal-to-noise power ratio (SNR), and the gain is in proportion to the spreading factor. However, designing such low rate and powerful, near-capacity achieving codes that is suitable for IDMA and can be decoded without imposing heavy computational complexity, has long been a bottleneck. A quantitative comparison between an intermediate solution (which is a combined use of a convolutional code and a low rate repetition code) and conventional CDMA (where error correction coding and spreading are independently performed) is made by [9]. In [10], it has been shown that IDMA with non-Gray (natural) mapping rules achieves better performance than with the Gray mapping, and such tendency is verified by the the *extrinsic* information transfer (EXIT) analysis. However, the bit error rate (BER) curves with the technique shown in [10] exhibits an error-floor because of not well matched EXIT curves.

Recently, a very excellent idea has been proposed in [11], which describes a technique that jointly optimize the mapping labeling rule and code parameters, resulting in very close matching of EXIT curves between the demapper and the decoder. The technique, EXIT-constrained binary switching algorithm (EBSA), uses extended mapping (EM) for modulation, which maps multiple labeling patterns to a single constellation point, and the code parameters are determined by using linear programming (LP) for code design; by repeating the code and labeling pattern design alternatively, very close matching of the EXIT curves can be achieved. In [11], the EBSA technique was applied to 4-quadrature amplitude modulation (4-QAM)-based bit interleaved coded modulation with iterative detection (BICM-ID), extended by 3 bits totaling 5 bits per symbol, where single parity check (SPC) and irregular repetition (IrR) code are used as the channel code. EBSA is found to be surprisingly powerful and flexible in jointly optimizing the parameters; it is shown in [11] that with spectral efficiencies of 1.0595 and 1.4501 bits/channel-use, the gaps to the Shannon limit with Gaussian codebook is 0.51 dB and 0.82 dB at BER of 10^{-5}, respectively, although the BICM-ID decoder requires computational complexity of only roughly 1/4 of the turbo code presented in [1]. Furthermore, error-floor is eliminated (or

at least reduce it to a value region below $10^{-6}-10^{-5}$ of BER). Inspired by the powerfulness and the high flexibility of the EBSA algorithm, the research on whether or not its near-capacity performance using BICM-ID and very low rate SPC-IrR codes is still effective when it is applied for IDMA has been invoked; the research interest includes BICM-ID-based IDMA systems design, performances analysis in the different type of channels, and verification of the sensitivity to frame-asynchronism.

1.2 Summary of Contributions

This research aims to analyze performances of an uplink IDMA, of which crucial requirement is the proper operability at a very low SINR range. In this research, a new IDMA system is built on the basis of BICM-ID principles with single user detection (SUD) and MUD, over additive white Gaussian noise (AWGN) channels and frequency selective fading channels. The EBSA optimization technique is applied to optimize the parameters of the transmission chain, which includes codes parameters and labeling patterns. Furthermore, the work related to future practical application such as power allocation and the impact of frame-asynchronism are also investigated. The main achievements of this thesis can be summarized as follows:

(i). The achievability of near-capacity performance of BICM-ID using very low rate SPC-IrR codes at a very low SINR range is demonstrated, and hence the technique is effective in achieving excellent performance when it is applied for IDMA. It is shown that EBSA can be used to optimize the parameters of the IDMA transmission chain.

(ii). Very simple SUD and MUD techniques, for the SPC-IrR BICM-ID IDMA which does not impose heavy per-iteration computational burden, are proposed in AWGN channels. Simulation results show the SUD techqiue can achieve near Shannon-capacity performance in AWGN channel, and the MUD technique in AWGN plus interference environment as well. Then, the impact of power allocation on the convergence property of MUD as well as on the MAC rate region has been evaluated by using the multi-dimensional EXIT chart and trajectory analyses. Furthermore, the impact of the frame-asynchronism is also investigated.

(iii). A joint turbo equalization and BICM-ID-based IDMA technique over frequency selective fading channels has been proposed. A frequency domain soft-interference cancelation minimum mean-square error (FD-SC-MMSE) turbo equalization is used for IDMA signal detection, where soft-interference cancelation takes place jointly with FD-SC-MMSE to detect all the simultaneous users. Simulation results show that the proposed technique

can eliminate the influences of both ISI and MAI, due to, respectively, the fading frequency selectivity and the channel sharing with other simultaneous users, and achieve the excellent frame error rate (FER) performance in single, 8 and 10 users' cases where in the 10 users' case, the user number is larger than its equivalent spreading factor. Then, a detection ordering (DO) technique is proposed to improve the efficiency of the detection scheme.

1.3 Thesis Outline

This thesis is organized as follows:

In **Chapter 1**, the research background and motivation are introduced. It is followed by the summary of contributions and outline of this thesis.

Chapter 2 reiviews the fundamental concepts of channels models, EXIT chart analysis and BICM-ID principle. Then, the system of SPC-IrR BICM-ID with EM and EBSA optimization is introduced.

Chapter 3 investigates IDMA systems based on BICM-ID principle and propose very simple SUD and MUD techniques without imposing heavy computational complexity. Then the impact of power allocation is investigated. The BER performances of the proposed IDMA system in AWGN channels are provided to show the near-capacity performances of in both the cases of SUD and MUD as well as in the case of with power allocation. After that, the impact of power allocation on the convergence and MAC rate region is analyzed. The last part of this chapter investigates IDMA in an asynchronous scenario. Simulation results shows that the proposed IDMA is very robust aganist frame-asynchronism.

Chapter 4 focuses on a joint turbo equalization and BICM-ID-based IDMA over frequency selective fading channels. The technique, composed of a FD-SC-MMSE turbo equalization together with IDMA signal detection to detect all the simultaneous users, can eliminate both MAI and ISI very efficiently. Simulation results show that the proposed joint turbo equalization and BICM-ID-based IDMA technique can achieve excellent FER performance. A DO techique which can determine the detection order of users is proposed to improve the efficiency of the system.

Chapter 6 summarizes this thesis with concluding statements and the future work.

Chapter 2

Preliminaries

In this chapter, some fundamental concepts as well as parts of the earlier work and techniques involved in this research are provided. First of all, the channel models including AWGN and frequency selective fading channels, as well as AWGN channel capacity and outage probability, are introduced. Then, the basic concept of EXIT analysis, which is used to evaluate the convergence property of the communication systems in the following charpters, is presented. Moreover, the principle of BICM-ID, which plays a key role in the proposed system, is provided for better understanding of this research. Finally, the proposed BICM-ID system with SPC-IrR codes and EM modulation as well as EBSA is explained in detail.

2.1 Channel Models

In telecommunications, a communication channel, refers to a physical transmission medium conveying the communicating information for one or several transmitters to one or several receivers. There are many types of models used to describe the statistical properties of the commnication channels. In this research, only static AWGN, and frequency flat and selective fading channels are used when evaluating the performance of the proposed systems. The channel's information transmission capability is liminted by a certain limit, usually measured by its data rate in bits per second or its bandwidth in Hz, such as AWGN channel capacity and outage probabilities of fading channels.

2.1.1 AWGN Channels

AWGN is a basic mathematical model describing noise. Basically, if the transmitted signal $\mathbf{x}$ is sent via the AWGN channel, a white Gaussian random noise variables $\mathbf{n}$ is added to $\mathbf{x}$. The received singal $\mathbf{r}$ can be expressed as

$$\mathbf{r} = \mathbf{x} + \mathbf{n}, \tag{2.1}$$

where the Gaussian random variables $\mathbf{n}$ are independent and identically distributed (i.i.d.) with a zero mean and a variance of $\sigma_n^2 = N_0/2$ per dimension. N_0 denotes the two-sided spectral density of the noise.

AWGN channel model doesn't take into account fading, frequency selectivity, nonlinearity and other channel properties. However, it provides very simple mathematical models which are useful for investigating the potential behavior of a system before considering the other natural phenomenon.

AWGN Channel Capacity

As stated by Shannon in [12], the channel capacity, the maximum number of bits per channel use or bits per dimension that could be correctly transmitted via a channel, is equal to the mutual infromation between the channel input and output, and the maximization is with respect to the input distribution $p(\mathbf{x})$, which is formulated by

$$C = \max_{p(\mathbf{x})} I(\mathbf{x}; \mathbf{r}). \tag{2.2}$$

Note that the transmitted signal $\mathbf{x}$ and the AWGN noise $\mathbf{n}$ are independent of each other.

According to Shannon's work, the channel capacity can be further expressed as

$$C = B\, log_2\,(1 + \gamma), \tag{2.3}$$

where B and γ are the bandwidth and the channel SNR, respectively.

In this research, the complex Gaussian channel is used where the AWGN is two-dimensionally distributed with the variance being $\sigma_n^2 = N_0/2$ in each dimension. In this case, the capacity can be deduced as

$$C = log_2\,(1 + \frac{E_s}{N_0}), \tag{2.4}$$

where E_s denotes the average energy per symbol with channel SNR being defined by $\frac{E_s}{N_0}$, if the receiver filter's Nyquist bandwidth B is equal to the inverse of the symbol duration.

2.1.2 Frequency Selective Fading Channels

In wireless communications, the transmitted signal is subjected to multipath propagation resulted from various types of obstacles such as deflection, scattering and reflection, which imposes variations in symbol amplitude and phase. This phenomenon is referred to as fading. In frequency selective fading channel, the channel coherence bandwidth is smaller than the bandwidth of the transmitted signal so that different frequency components of the signal experience different fading variations. Consider a frequency selective fading channels with L propagation paths. The received signal sequence at the receiver side can be expressed as

$$\mathbf{r} = \mathbf{H} \cdot \mathbf{x} + \mathbf{n}, \tag{2.5}$$

with the channel matrix

$$\mathbf{H} = \begin{bmatrix} h_1 & & & 0 \\ \vdots & h_1 & & \\ h_L & \vdots & \ddots & \\ & h_L & \vdots & h_1 \\ & & \ddots & \vdots \\ 0 & & & h_L \end{bmatrix}, \tag{2.6}$$

where $\mathbf{H} \in \mathbb{C}^{(M+L-1)\times M}$, M is the block length, and h_l, $l = 1, ..., L$, is the complex channel gain. h_l is modeled as i.i.d. zero mean random Gaussian processes. The channel frequency selectivity is due to multipath propagation. In this thesis, fading channel gains are constant over the transmitted coded data block duration, but vary block-by-block. This model is referred to as the block fading. Note that, if the channel is with a single path which is experiencing the block fading, it is referred to as frequency flat block fading channel. The received signal can be expressed accordingly as

$$\mathbf{r} = h \cdot \mathbf{x} + \mathbf{n}, \tag{2.7}$$

where h is the complex channel gain.

Outage Probability

The practical channels usually vary in time, and hence Shannon's channel capacity may become smaller than the channel code rate when the channels experience deep fade. The outage probability is introduced to express the statistical capability of the time-varying channels. Outage probability P_{out} is a standard performance criterion of communication systems for fading channels [13], and it is defined as the probability that the instantaneous SNR γ becames smaller than a specified threshold γ_{th} corresponding the rate to the channel code used. The outage probability is expressed by

$$P_{out} = P[0 \leq \gamma \leq \gamma_{th}] = \int_0^{\gamma_{th}} P_\gamma d\gamma, \tag{2.8}$$

where $p_\gamma(\gamma)$ is the probability density function (pdf) of γ. P_{out} can also be seen as the cumulative distribution function (cdf) of γ evaluated at γ_{th}.

2.2 EXIT Analysis

EXIT chart, a technique to design good iteratively-decodable error-correcting codes (in particular turbo codes), was developed by Stephan ten Brink on the concept of the property analysis for the *extrinsic* information exchange [14, 15]. It is an important tool to analyze the communication system, to optimize the coding and modulation chain as well as to better understand the convergence property of iterative decoding process.

If there are two components exchanging the *extrinsic* information, the behaviour of the components can be represented by a two-dimensional (2D) chart. If there are more than two components, the convergence behavior can be investigated by a three-dimensional (3D) chart. In the 2D'case, input *a priori* mutual information of one component is plotted on the horizontal axis and its output on the vertical axis. For the other component, its output *extrinsic* mutual information is plotted on the horizontal axis and its input *a priori* mutual information on the vertical axis. If the iterative decoding process is successful, the tunnel between the two curves is open so that the decoder can achieve the *a posteriori* mutual information very close to 1. EXIT chart can predict the position in the SNR value at which turbo cliff happens, the SNR value of which the tunnel opens until (1.0, 1.0) mutual information point. It should be noted that if the full mutual information (mutual information=1) can not be strictly achieved in practical scenarios, the error can not be fully eliminated, and there usually appears visible error floor in the performance curves. In practice, however, if the error floor is lower than, say, $10^{-6} - 10^{-5}$, no significant

degradation in the communication quality is expected.

The convergence property of the iterative decoding system can be visualized based on the EXIT chart. Moreover, the real behavior of the *extrinsic* mutual information exchange in realistic decoding process can also be visualized by a decoding trajectory. Furthermore, with the aid of the EXIT chart, the optimization of the codes design is turned into the problem of the shape matching between the EXIT curves of the inner and outer components. The optimization on codes and modulation labeling patterns, which plays an important role in this research, will be introduced in section 2.3.

2.2.1 Entropy and Mutual Information

In Information Theory, entropy is defined as a measure of the uncertainty or ambiguity of a random variable. The concept of entropy was first introduced in Shannon's landmark paper [12], which provides an absolute limit on the best possible lossless encoding or compression for any types of communications. Let X, be an i.i.d. discrete random varible with alphabet χ and probability mass function $p(x) = Pr\{X = x\}$, $x \in \chi$. The definition of the entropy [16], for a discrete random variable X, is defined by

$$H(X) = -\sum_{x \in \chi} p(x) \log p(x). \tag{2.9}$$

Entropy is expressed in bits if the log is to the base 2. $0 \log 0 = 0$ to be used as the convention for the completion of the definition, and $H(X)$ is non-negative.

The definition of entropy can be extended to a pair of discrete random variables X and Y with a joint distribution $p(x, y)$. The joint entropy of X and Y can be expressed as

$$H(X, Y) = -\sum_{x \in \chi} \sum_{y \in \mathfrak{Y}} p(x, y) \log p(x, y). \tag{2.10}$$

The conditional entropy of a random variable X given Y is defined as

$$\begin{aligned} H(Y|X) &= -\sum_{x \in \chi} p(x)\, H(Y|X = x) && (2.11)\\ &= -\sum_{x \in \chi} p(x) \sum_{y \in \mathfrak{Y}} p(y|x) \log p(y|x) && (2.12)\\ &= -\sum_{x \in \chi} \sum_{y \in \mathfrak{Y}} p(x, y) \log p(y|x) && (2.13)\\ &= -E \log p(Y|X). && (2.14) \end{aligned}$$

The relationship between the definitions of joint entropy and conditional entropy is that the entropy of a pair of random variables is the entropy of one random variable plus the conditional entropy of the other, which is known as the chain rule, expressed by

$$H(X,Y) = H(X) + H(Y|X) \tag{2.15}$$
$$= H(Y) + H(X|Y). \tag{2.16}$$

A measure of the mutual dependence of two random variables is defined as the mutual information, which is the relative entropy between the joint distribution and the product distribution $p(x)\,p(y)$, expressed as

$$I(X;Y) = -\sum_{x\in\chi}\sum_{y\in\mathfrak{Y}} p(x,y)\log\frac{p(x,y)}{p(x)\,p(y)}. \tag{2.17}$$

The mutual information decribes the reduction in the uncertainty of X by having the knowledge of Y. In summary, the connection between entropy and mutual information can be expressed by

$$I(X;Y) = H(X) - H(X|Y). \tag{2.18}$$

2.2.2 EXIT Chart

In order to better understand the principle of EXIT chart, a simple serially concatenated coding and iterative decoding process is considered, as shown in Fig. 2.1. The information exchange between the inner and outer decoders is in the form of soft log likelihood ratio (LLR). Since a random interleaver and its corresponding deinterleaver are placed between inner decoder and outer decoder, the output LLRs of both decoders can be considered as being uncorrelated to each other over many iterations. If the pdf of the *extrinsic* LLRs is approximated by a Gaussian-like distribution as the number of iterations increases [15, 17], the *extrinsic* LLRs is modeled as output of the equivalent Gaussian channel, where the known transmitted information bit x is assumed to suffer from zero mean Gaussian noise n_l with varince σ_l^2. The LLRs can then be expressed as

$$L = \eta_l\, x + n_l, \tag{2.19}$$

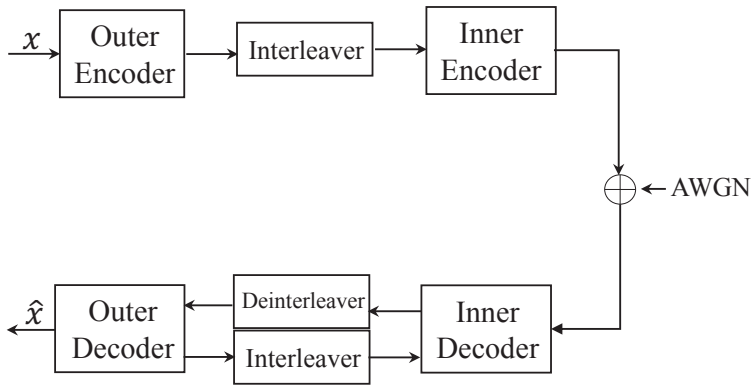

Figure 2.1: The system model with a simple serially concatenated coding and iterative decoding structure.

with $\eta_l = 2/\sigma_n^2$ and $\sigma_l = 4/\sigma_n^2$ denoting the mean and variance of Gaussian distributed equivalent noise n_l, respectively, where σ_n^2 is the variance of the AWGN of the real channel. The input of the inner decoder is the received signal from the AWGN channel and the *extrinsic* information of the outer decoder, while the output of the inner decoder is generated from the received signals and the *extrinsic* infromation from the outer decoder.

Base on (2.19) and recall that L is Gaussian distributed, the conditional pdf of the LLRs L is given by

$$p(l|x) = \frac{1}{\sqrt{2\pi}\sigma_l}\exp[-\frac{(l-\sigma_l^2 x/2)^2}{2\sigma_l^2}]. \tag{2.20}$$

Since LLR takes a continuous random value, we can use the general definition in (2.17) to measure the mutual information $I(X;L)$ between transmitted bits x and the LLRs l, which is calculated as

$$I(L|X) = \frac{1}{2}\sum_{x=+1,-1}\int_{-\infty}^{+\infty} p(l|x)\log_2\frac{2p(l|x)}{p(l|x=+1)+p(l|x=-1)}\,dl. \tag{2.21}$$

where x and l are the realizations of the random variables X of the transmitted bits and the corresponding LLRs, respectively.

Furthermore, the symmetry and consistency properties of $p(l|x)$ can be applied to avoid integration in (2.21), which are shown as

$$p(-l|x=+1) = p(l|x=-1), \tag{2.22}$$

and

$$p(-l|x=+1) = e^{l} \cdot p(l|x=+1), \tag{2.23}$$

respectively,

$$p(l|x=-1) = e^{l} \cdot p(l|x=+1). \tag{2.24}$$

Therefore, with the equations (2.21) to (2.24), the mutual information $I(X;L)$ can be approximated as

$$\begin{aligned} I(X;L) &= 1 - \int_{-\infty}^{+\infty} p(l|x=-1)\log_2(1+e^{-l})\,dl & (2.25)\\ &= 1 - E[\log_2(1+e^{-l})|x=-1] & (2.26)\\ &\approx 1 - \frac{1}{N}\sum_{i=1}^{N}\log_2(1+e^{-x_i l_i}). & (2.27) \end{aligned}$$

In [15], it is found that the mutual information $I(X;L)$ is a function of σ_l, which is referred to as J-function. The J-function shows the relationship between the mutual information and the variance as

$$J(\sigma) = I(\sigma_l = \sigma), \tag{2.28}$$

with

$$\lim_{\sigma\to 0} J(\sigma) = 0, \text{ and } \lim_{\sigma\to\infty} J(\sigma) = 1,\ \sigma > 0. \tag{2.29}$$

For binary signal transmission over Gaussian channels, the J-function can be approximated by

$$J(\sigma) \approx (1 - 2^{-H_1\sigma^{2H_2}})^{H_3}, \tag{2.30}$$

and

$$J^{-1}(I) = (-\frac{1}{H_1}\log_2(1 - I^{\frac{1}{H_3}}))^{\frac{1}{2H_2}}, \tag{2.31}$$

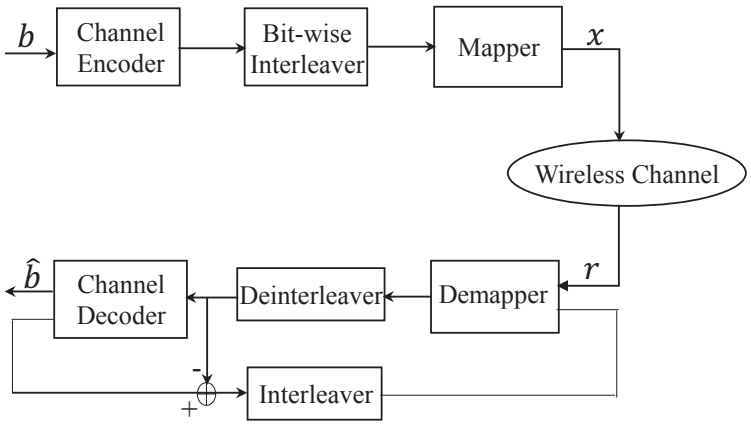

Figure 2.2: General structure of BICM-ID scheme.

with H_1, H_2 and H_3 being equal to 0.3073, 0.8935 and 1.1064, respectively, which were obtained by least square curve fitting [18]. The $J(\sigma)$ and $J^{-1}(I)$ functions convert the square-root variance σ_l of LLRs to mutual information, and vice versa, respectively.

2.3 SPC-IrR BICM-ID with Extended Mapping

The concept of Bit-interleaved Coded Modulation (BICM) was first proposed in [19] by Zehavi in 1992, of which the purpose is to increase the diversity order of the Trellis-coded-modulation (TCM) [20]. BICM renders the diversity order of the code equal to the number of different bits, rather than that of the differernt channel symbols by employing bit-wise interleaving. Then, BICM with iterative decoding (BICM-ID) was proposed in [21, 22] for further improving the BICM scheme, by eliminating the necessity of set partitioning based constellation labeling for TCM-turbo code, with the aim of the binary-level soft-decision-based information exchange between the demapper and decoder. Since BICM-ID can achieve high spectrum efficiency in AWGN channel, as well as path-diversity gain in frequency selective fading channels, it has been considered as one of the most promising candidates for the wireless access technology of future wireless communications systems.

2.3.1 BICM-ID Principle

The general structure of BICM-ID scheme is shown in Fig. 2.2. At the transmitter side, it is composed of a serial concatenation of channel encoder, bit-wise interleaver, and mapper that maps a certain length vector of the interleaved bit segment on to a modulation-signal

point. The source information bits b are processed by the transmitter chain, described above, and transmitted to the wireless channel as a symbol sequence x with a specified mapping rule. At the receiver side, the received signal r comprises transmitted symbol x suffering from the channel properties including AWGN, as described in section 2.1. The iterative detection and decoding process, which follows the turbo principle [1], is applied to improve the performance of the system. The exchanged information between demapper and channel decoder is in the form of *extrinsic* LLRs.

In the iterative process, interleaver and deinterleaver play a very important role. The *extrinsic* LLRs of the coded bits from the channel decoder are interleaved and fed back to the demapper where it is used as *a priori* LLRs to help the demapping process. On the other hand, the demapper output extrinic LLRs are deinterleaved and input to the decoder to help the decoding process. Such iterative process is repeated until there is no significant increase of *a posteriori* mutual information in the decoding process. Finally, channel decoder makes hard decision based on *a posteriori* LLRs of the systematic bits and outputs $\hat{b}$. Through iterative process, the demapper obtains the knowledge of the coded bits in the form of *a priori* LLRs, and generate the *extrinsic* LLRs to be passed to the channel decoder to improve the reliability.

It should be noted that since the BICM-ID performance is the matter of the matching of the demapper and decoder's EXIT curves, mapping rule also plays a crucial role of determining the performance.

This research applys the near-Shannon capacity achieving BICM-ID structure proposed in [11, 23, 24], which is depicted in Figs. 2.3. This system uses very simple codes, SPC-IrR codes, followed by Doped Accumulator (DACC) and combined with 4-QAM EM for modulation, where the transmitter structure is shown in Fig. 2.3(a). First of all, the source information bit sequence b_i, at the timing index i, is encoded by SPC-IrR encoder, and then interleaved, encoded by DACC to generate a new bits sequence u_j, and a vector with a certain length of the interleaved bit sequence is mapped to symbol x_m with 4-QAM EM modulation. Channel is assumed to be suffering from AWGN. In the receiver part, the process on demapping of EM and decoding of SPC-IrR are performed iteratively to detect the received signal r_m, based on the turbo principle with the help of interleaver and deinterleaver, as shown in Fig. 2.3(b). The exchanged information between demapper and decoder, indicated by EM^{-1} and $\mathrm{SPC}^{-1}\mathrm{IrR}^{-1}$, respectively, are in the form of *extrinsic* LLRs. Finally, the hard decision is made to obtain the final decoder's output $\hat{b}_i$. The components of the transmitter and receiver parts are introduced one by one in the following subsections of this section.

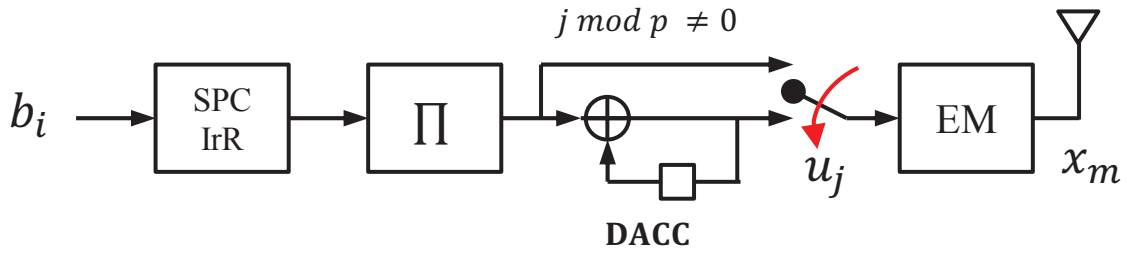

(a) The transmitter structure

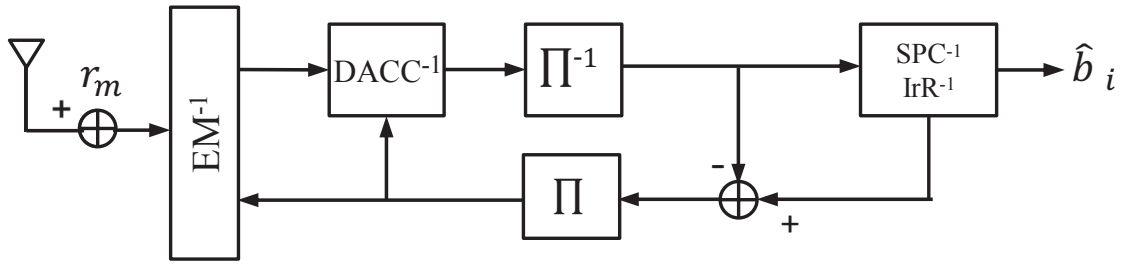

(b) The receiver structure

Figure 2.3: The proposed BICM-ID system structure.

2.3.2 Single Parity Check and Irregular Repetition Codes

In conventional BICM-ID, convolutional code is usually used for channel encoding. However, in this research, it uses very simple codes, SPC and IrR codes, in which the key role is the design of check node degree as well as degree allocation for variable nodes in irregular repetition code. Although the SPC-IrR code itself is very weak, but it is suitable when optimizing the parameters to match the demapper and decoder's EXIT curves, which will be introduced in 2.3.7.

SPC Code

Based on single parity check rule, a single parity check bit is added to every $(d_c - 1)$ source information bits, where d_c is defined as the check node degree.

IrR Code

IrR is a repetition code satisfying the specified irregular degree allocations, which indicates that the uncoded bit sequence is repeated specific times according to the variable node degree $\mathbf{d}_v$ and their corresponding ratio $\mathbf{a}$.

SPC-IrR Encoding Example

The structure of SPC-IrR encoder is shown in Fig. 2.4, where a very simple example of the SPC-IrR encoding process is also provided. In this example, the information bit sequence is first encoded by SPC encoder with the check node degree $d_c = 5$, i.e., one check bit is added after every 4 information bits. Then, the SPC coded bits sequence is further encoded by IrR encoder, where the variable node degree $\mathbf{d_v} = \{2, 3\}$ and the corresponding ratios $\mathbf{a} = \{0.4, 0.6\}$, thus, the 40% of the SPC coded bits are repeated by 2 times and the rest 60% of the bits are repeated by 3 times.

The rate of the SPC-IrR codes can be calculated by

$$R = \frac{d_c - 1}{d_c \cdot (\mathbf{d_v} \cdot \mathbf{a}^T)}, \tag{2.32}$$

and the spectrum efficiency can be calculated by

$$\eta = l_{map} \cdot R \tag{2.33}$$

$$= \frac{l_{map} \cdot (d_c - 1)}{d_c \cdot (\mathbf{d_v} \cdot \mathbf{a}^T)}, \tag{2.34}$$

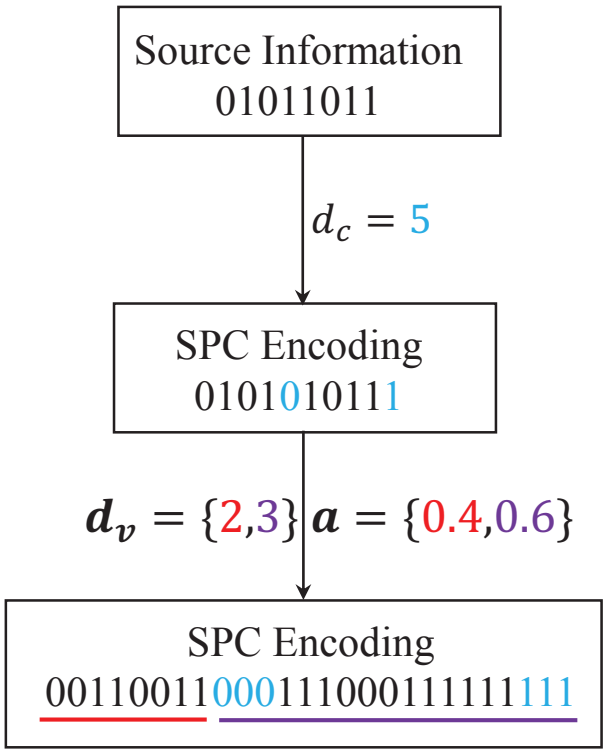

Figure 2.4: Encoding structure of SPC-IrR encoder.

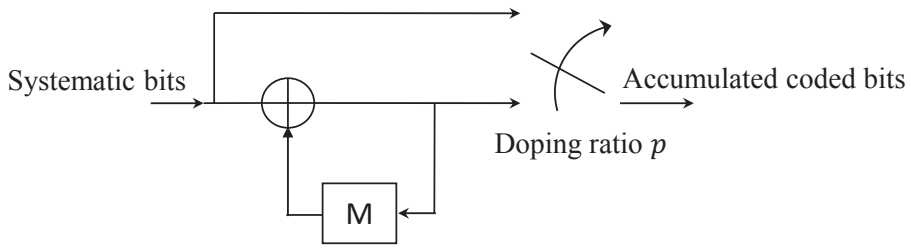

Figure 2.5: The structure of doped accumulator.

with l_{map} representing the number of bits per symbol in the modulation scheme.

2.3.3 Interleaver and Deinterleaver

Originally, interleaver was introduced to enhance the performance of error correction by permutating the order of the source bits sequence in the stream, while deinterleaver performs the inverse process to recover the order of the permutated bits. Interleaver and deinterleaver is conventionally used to spread the burst errors caused by the channel so that the error probability of a certain bit can be independent with that of the neighbouring bits.

However, in BICM-ID scheme, interleaver is utilized to make the randomness of the code, which follows the random coding concept, as in turbo codes on low density parity check (LDPC) codes. In other words, interleaving and deinterleaving are used to reduce the correlation of the LLRs so that decoding and demapping processes can be performed independently without making any influence to each other. In this thesis, it is assumed that the length of the interleaver and deinterleaver is the same as the length of coded bits sequence, even though interleaving over multiple block of sequences may further randomize the code structure. This is left as a future study.

2.3.4 Doped Accumulator

The structure of Doped Accumulator (DACC) is the same as the memory-1 recursive systematic convolutional codes, which is shown in Fig.2.5. In DACC, the output is a mixture of systematic bits and the accumulated coded bits. In the encoding process, every P-th systematic bits is replaced by the accumulated coded bits. It should be noted that the code rate of DACC is 1 because it does not change the overall code rate. The aim of applying DACC in this research is to push up the right most part of the inner code's

EXIT curve close enough to the (1,1) mutual information point, so that the error floor in the BER performance can be eliminated in the visible value range such as $10^{-6} - 10^{-5}$.

2.3.5 Mapping

In telecommunications, the process of modulation is to convert the logical information sequence into physical signal sequence that can be transmitted over the channels. QAM, based on two orthogonal carriers for amplitude modulation, is one of the modulation models which has been widely used in wireless communications, where the constellation diagram plays a very important role as a useful representation of the signals. The signal points are assigned to follow the constellation diagram, while the labeling patterns are determined by the mapping rule.

In the process of modulation, the constellation exhibits the signal as a 2D diagram in the complex plane. The modulation forms which are widely used are 4-QAM, 16-QAM, 32-QAM, and in general, 2^W-QAM (W represents bits per symbol), since in digital communications, the information sequence is usually binary, the number of points in the grid is usually a power of 2. In this research, the 4-QAM is used, in which standard mapping and EM are considered.

4-QAM Standard Mapping

In the constellation diagram of 4-QAM, the standard mapping rule is that 2 bits are mapped to each transmitted symbol. There are two types of 4-QAM mapping rule, Gray mapping and non-Gray mapping, which are referred to as 4-QAM standard mapping as shown in Figs. 2.6. Note that with the full *a priori* information of one bit, the other bit can be detected by comparing the Euclidean distances between the two selected constellation points. The following observation should be emphasized regarding the difference between the Gray and non-Gray mapping rules [20]:

- 4-QAM Gray standard mapping constellation is shown in Fig. 2.6(a). It is found that, determining the first bit is not affected by the knowledge of the second bit, and the Euclidean distances stay the same which is 2; determining the second bit is not affected by the knowledge of the first bit, either.

- 4-QAM non-Gray mapping constellation is shown in Fig. 2.6(b), where it is found that determining the first bit is affected by the knowledge of the second bit, and

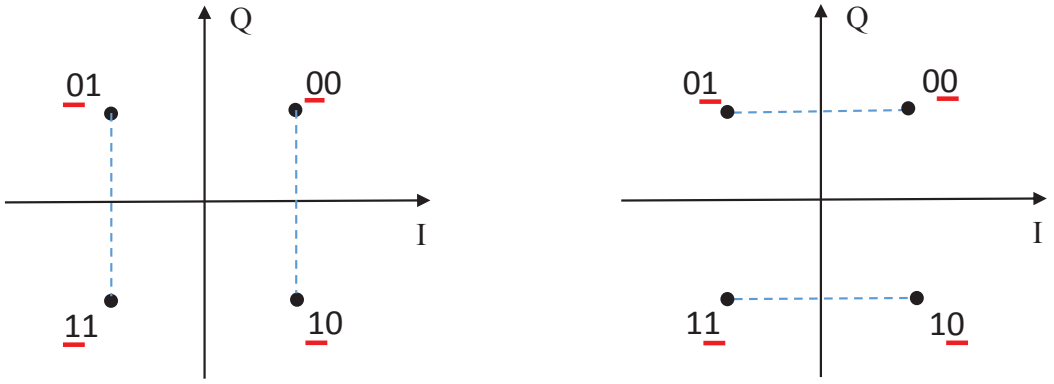

(a) Gray mapping

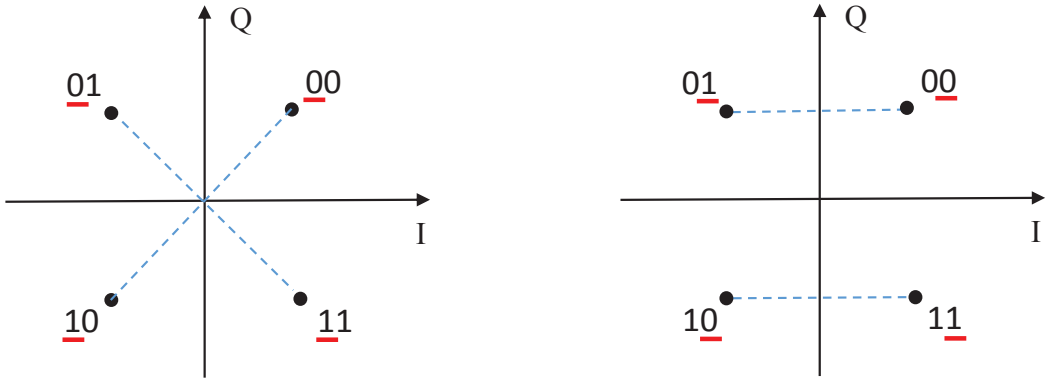

(b) Non-gray mapping

Figure 2.6: 4-QAM standard mapping.

with the full knowledge of the second bit, the Euclidean distance to be compared is $2\sqrt{2}$. Obviously, it is larger than with Gray mapping.

4-QAM Extended Mapping

The Extended Mapping (EM) concept was deeply investigated in [25] by Patrick Henkel, of which the aim is to increase the length of the labeling map for a given constellation. With EM technique, more than one labels having different bit patterns in the segment are mapped on to each constellation point, which indicates l_{map} bits are mapped on to a constellation point for modulation. l_{map} is assumed to be the number of bits per symbol, which can be expressed as

$$l_{map} = \log_2 W + e, \tag{2.35}$$

with e is the number of the extended bits.

There are two examples shown in Figs. 2.7, where 3 bits (2 labelings) and 4 bits (4 labelings) are mapped on to each symbol (constellation point), indicating by $l_{map} = 3$ and $l_{map} = 4$ with the number of extended bits 1 and 2, respectively. It is found that there are many possible combinations of bit patterns to be allocated to each constellation points. However, in iterative demapping and decoding schemes, with *a priori* information, the ambiguity of the mapping can be reduced by combining a certain outer coding process. The optimization of the extended mapping with *a priori* information has been taken into account in this research, aiming to maximize the Hamming distance between all the labels at each constellation point as well as the Hamming distance between each of the neighboring signal points. The detail of the optimization on extended mapping is explained in subsection 2.3.7.

2.3.6 Demapper and Decoder

As described above, at the receiver part, the iterative process is performed, where *extrinsic* information is exchanged between the demapper and decoder. Since the signal is transmitted over a AWGN channel, the discrete time description of the received signal r_m is expressed as

$$r_m = x_m + n_m, \tag{2.36}$$

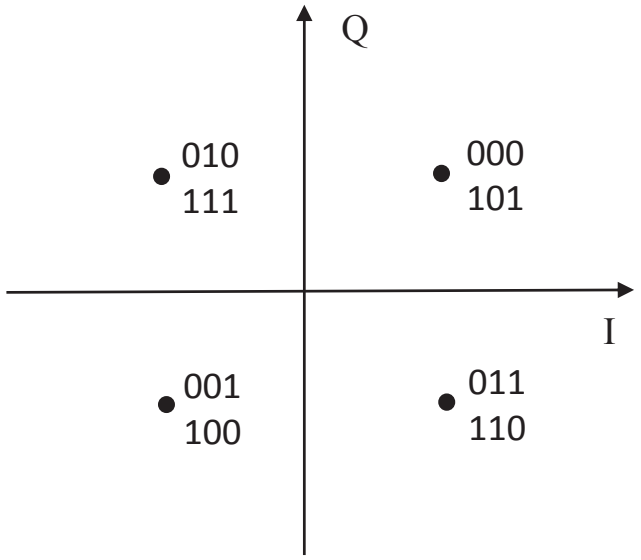

(a) $l_{map} = 3$

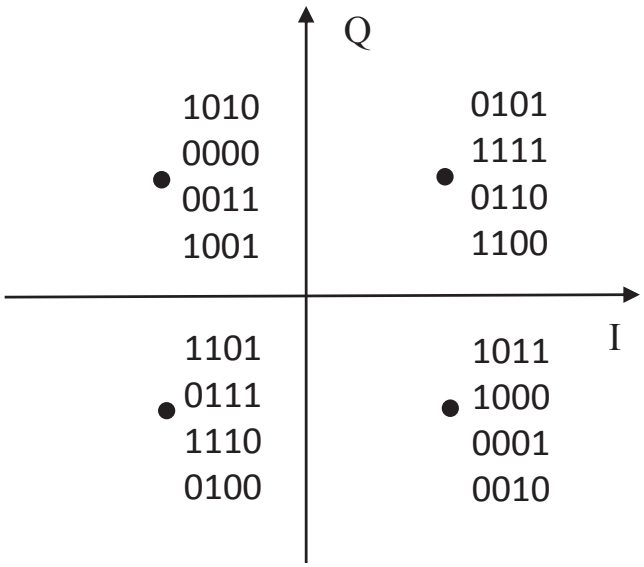

(b) $l_{map} = 4$

Figure 2.7: 4-QAM extended mapping.

where m and n_m denote the timing index and the zero mean complex AWGN component with variance σ_n^2, respectively.

Demapper

The received signal, together with the initial *a priori* LLRs $L_{a,dem}$ fed back from the decoder, are first sent to EM demapper. Based on maximum *a posteriori* probability algorithm (MAP), the *extrinsic* LLRs $L_{e,dem}$ of the demapper output of the d_{th} bit in the labeling vector corresponding to the transmitted symbol can be expressed as

$$L_{e,dem}[b_d] = \ln \frac{\sum_{x_m \in S_0} e^{-\frac{|r_m - x_m|^2}{\sigma_n^2}} \prod_{q=1, q\neq d}^{\ell} e^{-b_q(s) L_{a,dem}(b_q(s))}}{\sum_{x_m \in S_1} e^{-\frac{|r_m - x_m|^2}{\sigma_n^2}} \prod_{q=1, q\neq d}^{\ell} e^{-b_q(s) L_{a,dem}(b_q(s))}}, \tag{2.37}$$

where $S_0(S_1)$ and $L_{a,dem}(b_q(s))$ denote the labeling set, of which the d-th bit is 0(1), and the *a priori* LLR, fed back from the decoder, corresponding to the q_{th} position in the label allocated to the signal point s, respectively. q indicates the position of the bits allocated in the symbol x_m. $L_{a,dem}$ is equivalent to *extrinsic* LLR $L_{e,dec}$ of the decoder forwarded via the deinterleaver.

Decoder

After EM demapping, the output *extrinsic* LLRs $L_{e,dem}$ of demapper are sent to the DACC decoder, indicated by DACC^{-1} in Fig. 2.3(b). Since DACC uses memory-1 rate-1 recursive systematic convolutional code, the Bahl-Cocke-Jelinek-Raviv (BCJR) algorithm is performed for the DACC^{-1} [26]. Then, the output of DACC^{-1} is deinterleaved and used as *a priori* LLRs $L_{a,dec}$ of the SPC-IrR decoder. Since the variable node degrees d_{v_i} of the irregular code structure have different values segment-by-segment, the process of SPC-IrR decoding performs segment-wise accordingly. The detail of the SPC-IrR decoder as well as decoding algorithms are provided in [23, 27], therefore, only the summary of the decoding algorithm is provided here.

All the LLRs $L_{a,dec}$ corresponding to d_{v_i} bits are segmented, which are connected to a variable node, and d_c variable nodes are further connected to the corresponding check

node. The *extrinsic* LLR for a bit at the check node is updated as

$$L_{e,cnd,v} = 2 \arctan(\prod_{i=1,i\neq v}^{d_c} \tanh(\frac{L_{a,dec,i}}{2})), \tag{2.38}$$

where $L_{e,cnd,v}$ is the *extrinsic* LLR fed back to the v-th variable node. Then, it is combined with $(d_{v_i} - 1)$ *a priori* LLRs forwarded from the DACC^{-1} via the deinterleaver, as

$$L_{e,dec,v} = L_{e,cnd,v} + \sum_{w=1,w\neq v}^{d_{v_i}} L_{a,dec,w}, \tag{2.39}$$

This decoding process is invoked for the other bits in the same segment as well as for all the other segments independently in the same transmitted block. After finishing the processing for all the segments, the updated *extrinsic* LLRs of SPC-IrR decoder are interleaved and fed back to the EM demapper.

2.3.7 EXIT-constrained binary switching algorithm

EXIT-constrained binary switching algorithm (EBSA) is a novel framework proposed in [11] by Fukawa aiming to achieve near-Shannon capacity performance with the SPC-IrR BICM-ID EM system described above. EBSA [11] jointly optimizes the labeling pattern based on the binary switching algorithm (BSA) and node degree allocation utilizing linear programming (LP). With EBSA, the exact matching between the EXIT curves of demapper and decoder can be achieved while the convergence tunnel opens until the desired mutual information point. In this subsection, the framework of EBSA is briefly introduced, including design motivation and explaination of the roles of each components of the BICM-ID system described above.

Basic Principle

In serially concatenated systems such as BICM-ID, whether or not the system can achieve near-capacity performance depends on the matching between the EXIT curves of the inner and outer componets. It is well known that EXIT function is a non-decreasing function of *a priori* mutual information. In the case of BICM-ID, the EXIT curve of the demapper (including the decoder of DACC (DACC^{-1}, as indicated in Figs. 2.3). For the sake of notation simplicity, the terminology, demapper, indicates demapper-plus-DACC^{-1}

through out this thesis), which is the inner component, exhibits convex shape, i.e,

$$\frac{\partial^2 I_E(dem)}{\partial I_A^2(dem)} \geq 0, \quad 0 \leq I_A(dem) \leq 1.0, \tag{2.40}$$

where $I_E(dem)$ is the *extrinsic* MI between the demapper's output LLR and the transmitted coded bit, and $I_A(dem)$ is the *a priori* mutual information of the demapper. The EXIT curve of convolutional codes exhibits concave shape [9, 28] in a region where $I_A(dem)$ is relatively small, i.e,

$$\frac{\partial^2 I_A(dec)}{\partial I_E^2(dec)} \leq 0, \text{ for relatively small } I_A(dec), \tag{2.41}$$

where $I_E(dec)$ is the *extrinsic* mutual information between the decoder's output LLR and the transmitted coded bit, and $I_A(dec)$ is the *a priori* mutual information. Note that $I_A(dec) = I_E(dem)$ and $I_A(dem) = I_E(dec)$.

On the contrary, the EXIT curve of the SPC-IrR codes exhibits convex shape, i.e,

$$\frac{\partial^2 I_A(dec)}{\partial I_E^2(dec)} \geq 0, \quad 0 \leq I_A(dec) \leq 1.0. \tag{2.42}$$

According to the area property theorem [28], the area below the decoder's EXIT curve corresponds to the code rates, which requires the decoder's EXIT curve of the very low rate codes to exhibit a "reverse-L" shape. Obviously, since (2.40)–(2.42) indicate that to keep the convergence tunnel between the demapper and decoder's EXIT curves open until a point very close to the (1.0, 1.0) mutual information point in the EXIT chart, SPC-IrR is better suited to BICM-ID than convolutional codes. It should be noted here that if SPC is not used, the code used in this thesis is equivalent to non-systematic Repeat Accumulate (RA) code without check node encoder after interleaving. The role of SPC is to further push the EXIT curve of the decoder to the right side while not making significant change at the left side. Thereby, it is expected that the decoder's EXIT curve exhibits a "reverse-L" shape, by which the narrow tunnel opens until a point very close to the (1.0, 1.0) mutual information point.

In addition, the following two factors provide system design with more degrees-of-freedom: (1) because of the labeling extension with EM, the EXIT curve is further pushed downwards [27], even though the same physical constellation is used, and hence there exist some patterns which are suitable for low rate code design; (2) regardless of the labeling patterns and SNR values, DACC, the demapper's EXIT curve reaches a point very close

to the (1.0, 1.0) mutual information point.

As a whole, the designed BICM-ID system provides a basis of which parameters can be jointly optimized by EBSA, including the codes parameters and labeling pattern, which enable the system to achieve the near-capacity performance.

BSA Optimization

As described above, labeling pattern plays an important role on the performance of BICM-ID systems [25]. Several researches have proposed techniques to determine the optimal labeling pattern. BSA, which aims to optimize the labeling cost, are proposed in [29]. The BSA based labeling pattern optimization evaluates the labeling cost by assuming that full *a priori* information for the rest of the $(l_{map} - 1)$ bits are available. The cost function of each fixed label x^h in the constellation is given by

$$Z_{l_{map}-1} = \frac{1}{l_{map} 2^{l_{map}}} \sum_{v=1}^{l_{map}} \sum_{x^h | x_v^h = 0} \sum_{\hat{x_v^h} | \hat{x^h} = 1} \exp(-|\nu(\hat{x_v^h}) - \nu(\hat{x_v^h})|^2 / \sigma_n^2), \tag{2.43}$$

where function $\nu(\cdot)$ returns the constellation point corresponding to the labeling pattern x^h and $\hat{x^h}$ for the v-th bit being 0 and 1, with $h = 0, 1, ..., 2^{l_{map}-1}$.

The total cost function is a sum of the cost functions for each fixed symbol, as

$$Z_{l_{map}-1}^{total} = \sum_{h=0}^{2^{l_{map}-1}} Z_{l_{map}-1}^{h}. \tag{2.44}$$

The BSA is detailed as **Algorithm 3** in [11]. BSA is initialized by a random assignment of the labels to the symbols. The cost of each label and the total cost are calculated by (2.43) and (2.44) in each iteration (An iteration corresponds to the completion of a swap). Then, by comparing the total costs, the label with the highest cost is selected and a swap partner is searched when the decrease in total cost is maximized. If no suitable partner is found, the label with the second highest cost will be considered. This process is continued until a pair of the swap partner is found. The BSA is ended when there is no further reduction of the total cost in an iteration. Note that 100 random initializations of the BSA are sufficient to find the near global optimal labeling pattern.

LP Optimization

LP is a widely known method to find a solution to the problems represented by a linear combination of the optimization parameters and constant values. Recently, it was found that LP can be used to solve the problem of the optimal degree allocation for IrR code for the design of BICM-ID systems with the aim of achieving desired convergence property, as investigated in [24]. The optimal variable node degree allocations problems can be formulated as

$$\begin{aligned}
&\text{Minimize} \sum_{i=1}^{M} a_i d_{v_i} \\
&\text{Subject to} \\
&\sum_{i=1}^{M} a_i \; d_{v_i}(-J(\sqrt{(d_{v_i}-1)\; J^{-1}(I_{e,dem,w})^2 + J^{-1}(I_{e,cnd,w})^2}) \\
&, + I_{a,dem,w} + \epsilon_w) \;\leqslant 0 \;\; (\text{for } 1 \leqslant w \leqslant N) \\
&\sum_{i=1}^{M} a_i = 1
\end{aligned} \tag{2.45}$$

where N is the number of the indexes.

The other parameters appearing in (2.45) are shown as

$$I_{e,cnd} = 1 - J(\sqrt{d_c - 1} \cdot J^{-1}(1 - I_{a,cnd})), \tag{2.46}$$

with

$$I_{a,cnd} = J(\sqrt{d_v \cdot J^{-1}(I_{a,dec})^2}), \tag{2.47}$$

$$I_{e,dec} = J(\sqrt{(d_v - 1) \cdot J^{-1}(I_{a,dec}^2) + J^{-1}(I_{e,cnd})^2}), \tag{2.48}$$

and

$$I_{e,dec} = J(\sqrt{(dv - 1) \cdot J^{-1}(I_{a,dec}^2) + J^{-1}(I_{e,cnd})^2}). \tag{2.49}$$

Note that, $I_{a,dec} = I_{e,dem}$.

Furthemore, since the check node degree does not make any influence to the LP op-

timization, but it changes the code rate, a brute-force search is also performed to find the optimal check node degree, which is also summarized in **Algorithm 1** of [24]. This algorithm first initializes the variable node degree d_{v_i} and a_i, then with the fixed value range of d_c, the LP is performed to obtain optimal distribution a_i for each d_{v_i}. After that, the code rate R is calculated by using d_c, d_v and a_i. This process is repeated until all the d_c values in the given range for LP has been tested and the code rate calculated. Finally, the maximum code rate R is selected and the corresponding values of d_c, d_v and a are the optimal code parameters.

EBSA Framework

In the previous part of this subsection, the ideas of using BSA to optimize the EM labeling patterns combined with the LP optimization to obtain the optimal SPC-IrR code parameters, are briefly introduced. With the ideas, the framework of EBSA technique is proposed in [11], which aims to jointly optimize the labeling patterns, doping ratio of accumulator, and SPC-IrR code parameters. EBSA technique aims to minimize the gaps between the EXIT curves of demapper and decoder from both the vertical and horizontal directions. There is an example of demonstration of EBSA optimization shown in Figs. 2.8. Before the EBSA optimization, as shown in Fig. 2.8(a), there is a gap between the EXIT curves of the demapper and decoder, which indicates the rate loss. Furthermore, the two curves intersect before they reach the (1.0, 1.0) mutual information point, which indicates that turbo cliff can not be expected in the BER curve. However, after EBSA optimization, as shown in Fig. 2.8(b), the gap between the two curves is minimized in both the vertial and horizontal directions, using BSA and LP optimizations, respectively, so that a close matching can be achieved.

The framework of EBSA is proposed and summarized in **Algorithm 2** of [24], which first generates a gap-check vector and then repeat the following steps: (1) repeat the process, initializing the labeling pattern s randomly and performing BSA with the gap-check vector to obtain the lowest total cost sufficient times and selecting the labeling pattern which has the lowest total cost; (2) fix the doping ratio p a value range from 2, and for each doping ratio, perform LP optimization and calculate the code rate and finally determine the code parameters with the largest code rate; (3) compare the gap with the vertical and horizontal thresholds and change the gap-check vector accordingly. The process is teminated until the gap is smaller than both the vertical and horizontal thresholds, and the optimal parameters of SPC-IrR codes and doping ratio of accumulator as well as the optimal labeling pattern are obtained.

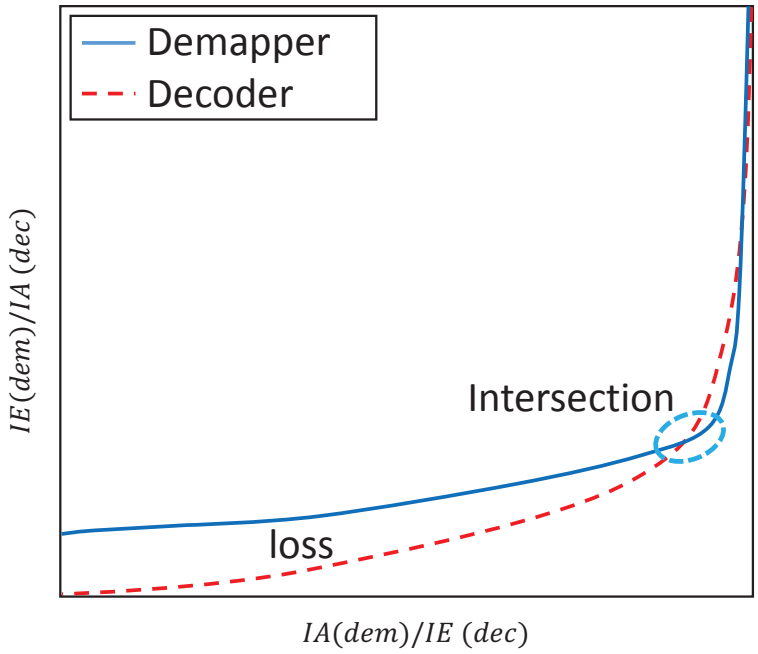

(a) Before EBSA optimization

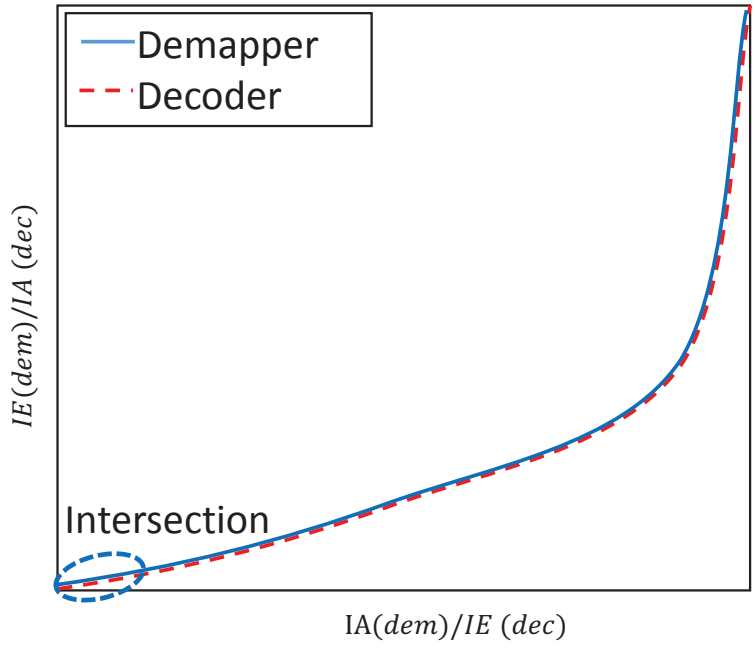

(b) After EBSA optimization

Figure 2.8: The demonstration of EBSA optimization.

Modulation Mixing

With the EBSA optimization, since the closing matching between EXIT curves of demapper and decoder can be achieved, the near-Shannon capacity BER performance is expected. We tested the algorithm operability and evaluate the BER performance, however, it is found that the iteration in the simulation can not start. In order to find the reason, the mutual information exchange was carefully observed on the EXIT curves with the optimal code parameters and labeling patterns obtained by EBSA. Finally, it is found that, becasue EBSA is very powerful, the EXIT curves are too close to each other at the very low mutual information point (near (0, 0) mutual information point as shown in Fig. 2.8(b)), and hence the tunnel does not open and the iteration can not start.

In order to solve this problem and flexibly control the shape of the EXIT curve of demapper, modulation mixing (MM) is used, which mixes the 4-QAM non-Gray standard mapping and EM in a certain ratio [30], for example, the mapping patterns are mixed at a certain ratio D ($D \times 100\%$ for 4-QAM non-Gray standard mapping and $(1-D) \times 100\%$ for 4-QAM EM, $0 \leqslant D \leqslant 1.0$). And the spectrum efficiency can be re-written by

$$\eta = [2 \cdot D + l_{map} \cdot (1 - D)] \cdot R \tag{2.50}$$

$$= \frac{[2 \cdot D + l_{map} \cdot (1 - D)] \cdot (d_c - 1)}{d_c \cdot (\mathbf{d_v} \cdot \mathbf{a}^T)}, \tag{2.51}$$

This technique lifts up the left-most point of the demapper's EXIT curve very slightly. Hence, EBSA optimization technique combined with MM can achieve close matching between the EXIT curves of demapper and decoder, while it can guarantee the opening of the convergence tunnel until the (1.0, 1.0) mutual information point, so that a turbo cliff is expected to happen at a near-capacity SNR value. Result of an example obtained by using EBSA combined with MM is shown in Fig. 2.9, where the very close matching between the two EXIT curves can be observed while the left-most point part is lifted up so that a very narrow tunnel is open entirely over the value range. After performing BER evaluation via simulation with the optimal parameters shown in a small box of Fig. 2.9, near-capacity performance is verfied; as shown in Fig. 2.10, a turbo cliff happens 0.51 dB away from the Shannon limit.

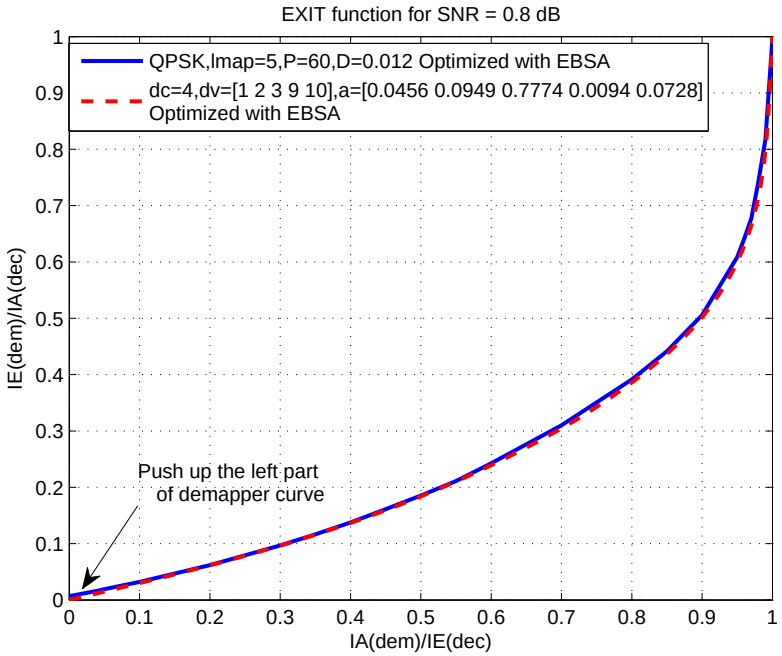

Figure 2.9: An example on EXIT chart with the results obtained by EBSA combined with MM technique.

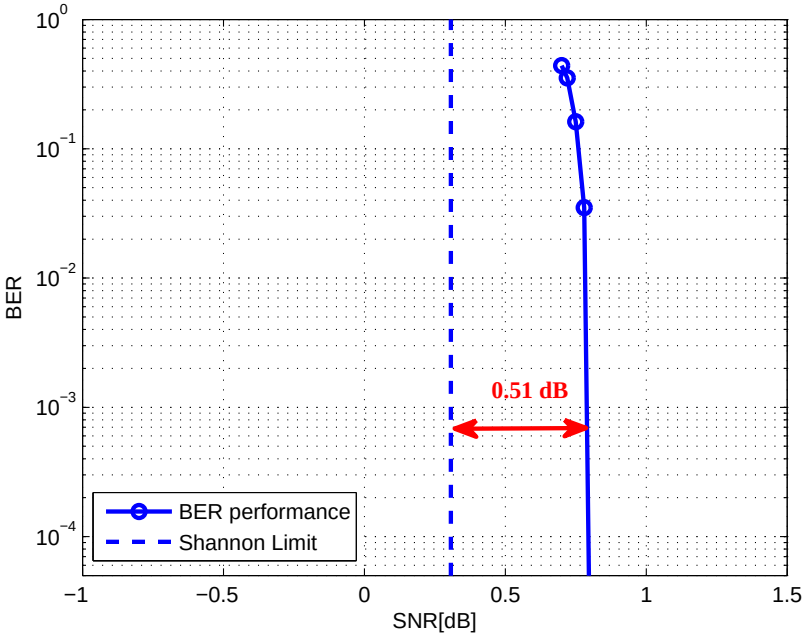

Figure 2.10: An example on BER performance of EBSA combined with MM technique.

2.4 Summary

In this chapter, some fundamental conceptual bases have been briefly introduced, such as channels models including AWGN channel, frequency selective fading channels, AWGN channel capacity, outage probability, and the basic concept of EXIT analysis. Moreover, several key techniques presented in the earlier work involved in this research, based on designing and optimizing BICM-ID system, are provided. The preliminary studies will be used in the main part of this thesis.

Chapter 3

BICM-ID-based IDMA

In this chapter, IDMA systems based on BICM-ID principle over AWGN channels is investigated. First of all, a brief description of the IDMA principle is provided. Then, the design of BICM-ID-based IDMA, with both SUD and MUD techniques, is presented to show the near-capacity BER performance in AWGN channels. After that, the power allocation is introduced, followed by the impact analysis of power allocation on the convergence and MAC rate region. Moreover, performance tendency of the proposed BICM-ID-based IDMA system in frame asynchronous scenario is also investigated in this chapter.

3.1 IDMA Principle

Nowadays, non-orthogonal Multiple Access (NOMA) has attracted a lot of attention with the aim of its application to the next generation broadband wireless communication systems, since the NOMA outperforms orthogonal signaling techniques in term of spectral efficiency advantage [31]. IDMA is a new proposed NOMA-based multiple access techniques, of which the original idea is inspired by Viterbi's work [4] and proposed in [5]. After that, the IDMA concept was reformulated and introduced in [6, 7] and [8]. Unlike CDMA system, which uses user-specific spreading sequence for user separation, IDMA employs interleavers for the users separation. It combines iterative joint detection and channel decoding to distinguish different users according to the turbo principle. Since IDMA has a variety of design flexibility and exhibits performance superiority, the use of the technique has been proposed for many applications and considered as one the most promising candidates for the uplink in future wireless communications.

The system model of the conventional IDMA is shown in Figs. 3.1, where the transmitter and the receiver parts are illustrated separately. The Fig. 3.1(a) shows the transmitter

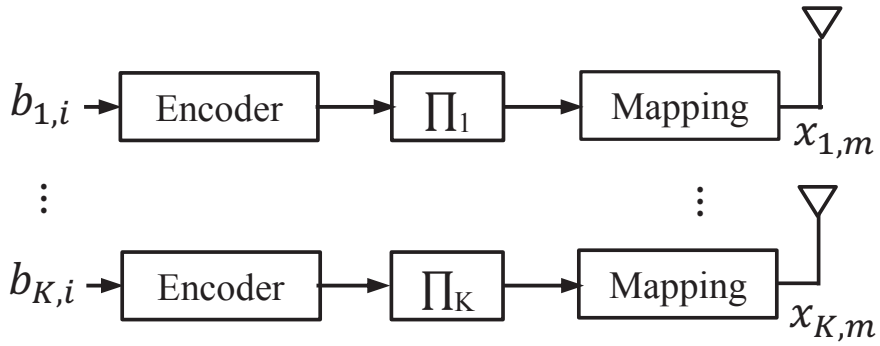

(a) The transmitter part

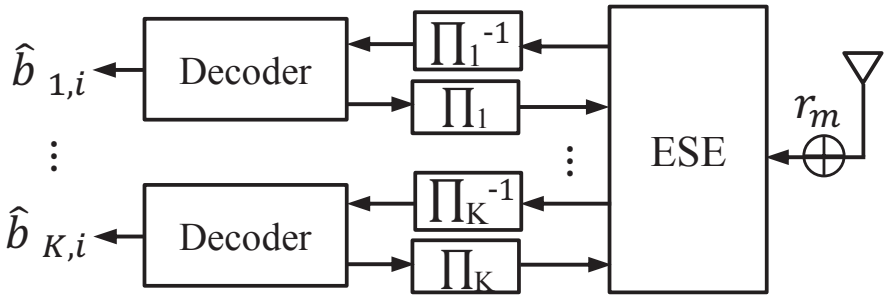

(b) The receiver part

Figure 3.1: The system model of conventional IDMA.

structure of the multiple access scheme under consideration with K simultaneous users. The input data $b_{k,i}$ (i denotes the time index of the users' original bit sequence) for user k-th is encoded by forward error control (FEC) encoder, bit-interleaved by random interleaver. Then, the coded bit sequence is modulated by the specific mapping rule so that each segment of the sequence is mapped to the symbol $x_{k,m}$ (m denotes the time index of the symbol sequence). After that, the modulated signal is transmitted through mutiple access channel.

At the receiver side, as shown in Fig. 3.1(b), the received signal r_m mixes all the users transmitted signals plus noise component, which can be expressed as

$$r_m = \sum_{k=1}^{K} x_{k,m} + n_m, \tag{3.1}$$

where n_m denotes the AWGN component with variance σ_n^2. However, when the k-th user is concentrated, the composite interference composed of the other users' signals can be seen as a part of the noise. Therefore, the received signal (3.1) can be rewritten as

$$r_m = x_{k,m} + \zeta_{k,m} \tag{3.2}$$

with

$$\zeta_{k,m} = \sum_{g=1,g\neq k}^{K} x_{g,m} + n_m, \tag{3.3}$$

where $\zeta_{k,m}$ indicates the MAI from the other users plus AWGN. It is assumed that $\zeta_{k,m}$ in (3.2) can be approximated by a Gaussian random variable. The information exchange between elementary signal estimator (ESE) and the each decoder is performed iteratively following the turbo concept.

In IDMA, the key principle is that the interleavers π_k should be different for each user. The interleavers are designed randomly and independently so that the interleaved simultaneous transmitted sequences are statistically independent.

Since, in IDMA, the bandwidth expansion is fully exploited for FEC coding that typically uses very low rate code, unlike in the CDMA systems. Based on the BICM-ID system design described in the last chapter, an idea of applying BICM-ID structure into IDMA system is arisen in [32], where it is found that the use of the BICM-ID technique [11] is very suitable for designing very low rate code achieving near-capacity performance. In the technique proposed in [11], the SPC-IrR code parameters, the DACC, the MM ratio,

and the labeling patterns for EM are optimized in a systematic way by using the EBSA technique in AWGN channels. EBSA optimizes SPC-IrR BICM-ID transmission chain that achieves close matching between the decoder and demapper's EXIT curves even in a very low SNR range. The use of the optimized SPC-IrR BICM-ID in IDMA systems has already been investigated in [32], where the excellent performance can be demonstrated via the convergence and rate region analyses. In the following sections of this chapter, the system design of the proposed BICM-ID-based IDMA, including the SUD and MUD techniques, is presented, together with the performance evaluation as well as the impact analysis of power allocation on convergence and rate region characteristics.

3.2 System Model

The system design of BICM-ID-based IDMA best utilizes the properties of BICM-ID scheme, a serial concatenation of channel coding and mapping, which requires low rate and near-capacity achieving codes. Since the performance of BICM-ID strongly depends on the matching between the constellation labeling pattern and the code structure, the code and mapping rule optimization technique described in the previous chapter provides an optimal solution to the design of the system. With the superiorities of the EBSA technique, the joint optimizations on codes and mapping of BICM-ID are feasible so that the designed BICM-ID scheme becomes well suited for applying to the IDMA system, which allocates the full bandwidth for channel coding.

The system model of the BICM-ID-based IDMA is depicted in Fig. 3.2, where at the receiver the iterative processing between the demapper and decoder is invoked user-by-user. The iterative detection process between demapper and decoder has two types of iterations: inner iteration and outer iteration. Inner iteration is activated independently for each user, while outer iteration is performed between different users. When the outer iteration is not involved in other users' signal detection, the system performs SUD; on the contrary, in MUD, the outer iteration is activated aiming to cancel the interference from the other users. Each user uses the same BICM-ID transmission structure, where the binary bit information $b_{k,i}$ of user-k, $k \in \{1, \cdots, K\}$, at the timing index i is SPC-IrR-encoded at the transmitter. The encoded bit sequence is bit-interleaved by a random interleaver Π_k, and then accumulated by DACC with the switching ratio p to generate a new bits sequence $u_{k,j}$, where j is the timing index at the output of DACC. The DACC output binary sequence $u_{k,j}$ are serial-to-parallel converted, and mapped on to a 4-QAM signal point, in part, according to the labeling pattern of EM, and in part, according

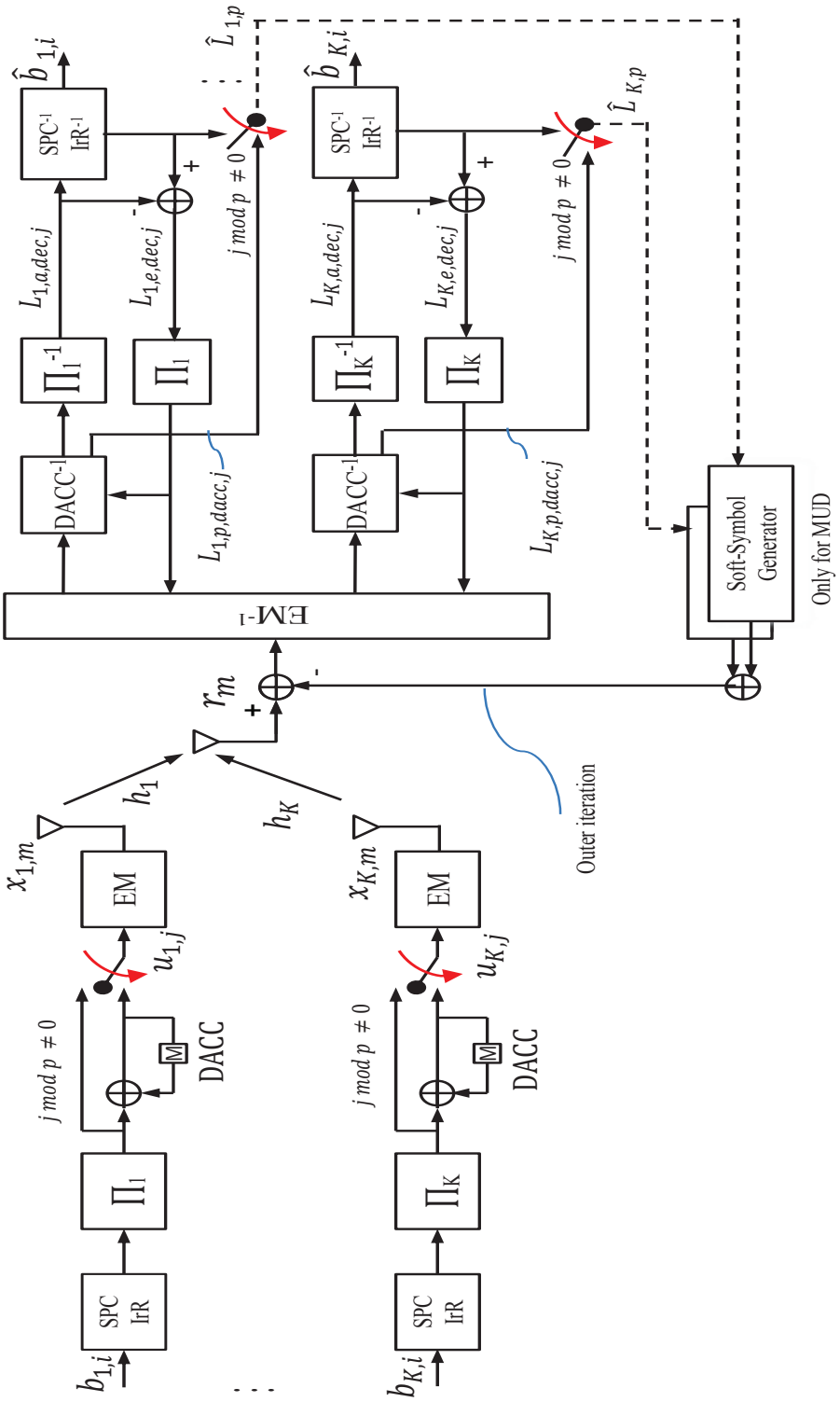

Figure 3.2: System model of the proposed BICM-ID-based IDMA system.

to the non-Gray labeling pattern to produce transmission symbols $x_{k,m}$ at the timing index m, with modulation mixing ratio D. After that, the transmission symbols $x_{k,m}$ are transmitted to the channel. With SUD, the receiver part detects each user independently, without the any help from the other users; however, with MUD, all the simultaneous users are to be detected jointly with the help of the other users in the form of soft cancelation.

3.3 Single User Detection

As described above, in IDMA systems, user separation is performed by the interleaver utilized in the iteratively decodable demapping and channel decoding system, for which its patterns have to be different user-by-user. Demapper for BICM-ID assumes that the other users are regarded as being equivalent to noise, and hence the demapper is purely a Single User Detection (SUD) detector. Then, the SUD detector works together with decoder so that each user is detected independently.

3.3.1 Detection Scheme of IDMA-SUD

In SUD, since at the receiver part of Fig. 3.2, the outer iteration is not activated, the received signal r_m at the timing index m can be expressed as

$$r_m = \sum_{k=1}^{K} \sqrt{P_k} \cdot x_{k,m} + n_m, \tag{3.4}$$

where P_k and n_m denote the power allocated to the k-th user and the AWGN component with variance σ_n^2, respectively. Each user's phase rotation is ignored in (3.4). This is only because of the simplicity, and in fact, as shown in Appendix for $K = 2$ which is the worst scenario, two cases were tested: one is the case where the phase rotations are ignored, and the other is the case with the phase rotation. They yield negligibly minor difference in demapper's EXIT curve. When concentrating on the k-th user, the composite interference composed of the other users' signals is equivalent to noise, and hence, (3.4) can be rewritten as

$$r_m = \sqrt{P_k} \cdot x_{k,m} + \zeta_{k,m} \tag{3.5}$$

with

$$\zeta_{k,m} = \sum_{g=1,g\neq k}^{K} \sqrt{P_g} \cdot x_{g,m} + n_m, \tag{3.6}$$

where $\zeta_{k,m}$ indicates the MAI from the other users plus AWGN. It is assumed that $\zeta_{k,m}$ in (3.5) can be approximated as a Gaussian random variable. Thus, the variance of interference plus noise, experienced by the k-th user, $\sigma^2_{k,\zeta}$, is expressed as

$$\sigma^2_{k,\zeta} = \sum_{g=1,g\neq k}^{K} P_g + \sigma^2_n, \tag{3.7}$$

where we assume $\mathbb{E}[|x_{g,m}|^2] = 1$.

The *extrinsic* information exchange between demapper and decoder is performed iteratively, at the receiver side, adhering the turbo principle. The *extrinsic* LLR $L_{k,e,dem}$ of the demapper output of the d-th bit in labeling vector corresponding to the transmitted symbol can be expressed as

$$L_{k,e,dem}[b_{k,d}] = \ln \frac{\sum_{x_{k,m}\in S_0} e^{-\frac{|r_m - x_{k,m}|^2}{\sigma^2_{k,\zeta}}} \prod_{q=1,q\neq d}^{\ell} e^{-b_q(s) L_{k,a,dem}(b_q(s))}}{\sum_{x_{k,m}\in S_1} e^{-\frac{|r_m - x_{k,m}|^2}{\sigma^2_{k,\zeta}}} \prod_{q=1,q\neq d}^{\ell} e^{-b_q(s) L_{k,a,dem}(b_q(s))}}, \tag{3.8}$$

where $S_0(S_1)$ and $L_{k,a,dem}(b_q(s))$ denote the labeling set, of which the d-th bit is 0(1), and the *a priori* LLR, fed back from the decoder, corresponding to the q-th position in the label allocated to the signal point s, respectively. $L_{k,a,dem}$ is equivalent to *extrinsic* LLR $L_{k,e,dec}$ of the decoder forwarded via the deinterleaver. q indicates the position of the bits allocated in the symbol $x_{k,m}$. The structure of the decoder as well as mathematical expressions for the decoder's *extrinsic* LLR calculation can be found in **Chapter 2**.

3.3.2 EXIT Analysis of IDMA-SUD

This subsection presents results of EXIT analysis for the proposed BICM-ID-based IDMA with SUD. We exactly follow the established methods [15, 28] when calculating the EXIT

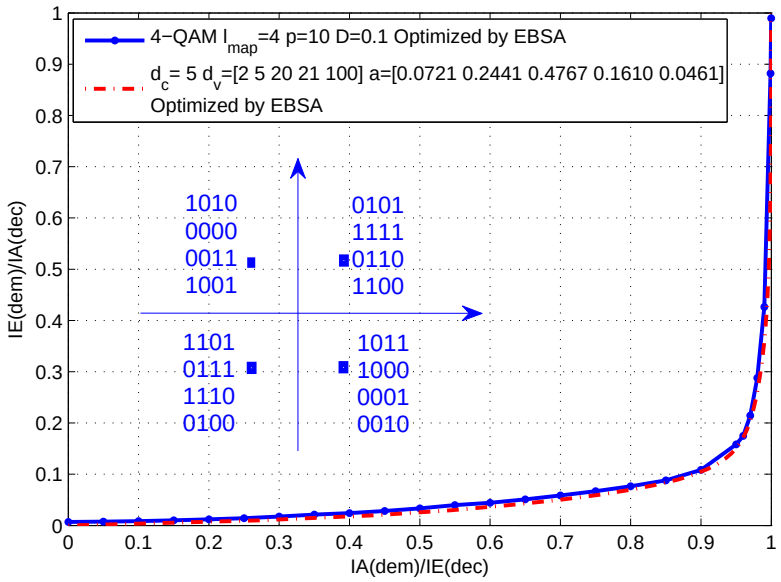

Figure 3.3: EXIT chart obtained as the result of EBSA at $SINR = -8.69$ dB (Code rate $R_c = 0.0424$, Spectrum efficiency $\eta_{\mathrm{SPC-IrR}} = 0.1611$ bits/4QAM-symbol).

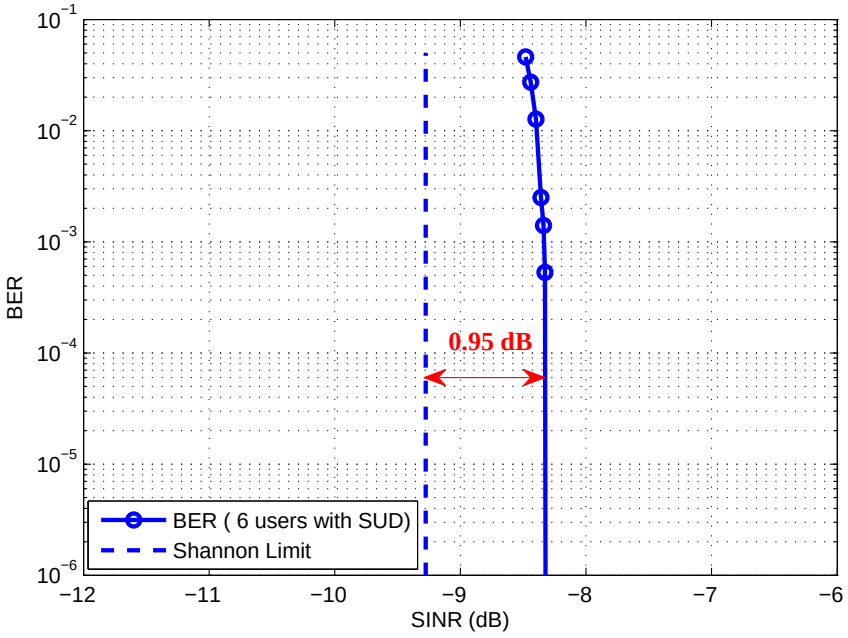

Figure 3.4: The BER peformance of IDMA-SUD with 6 users.

curves. SINR and SNR for each user are defined as follows

$$SINR_k = \frac{P_k}{\sum_{g=1,g\neq k}^{K} P_g + \sigma_n^2}, \tag{3.9}$$

$$SNR_k = \frac{P_k}{\sigma_n^2}, \tag{3.10}$$

where P_k, and σ_n^2 denote the power allocated to k-th user and AWGN noise variance, respectively.

Assume that the power allocated to each user is identical, i.e, $P_k = 1.0$. Fig. 3.3 shows the result of labeling pattern optimization for 2-bit extended 4-QAM ($l_{map} = 4$) with its demapper's and SPC-IrR decoder's EXIT curves; the labeling pattern and the code parameters were jointly optimized for spectrum efficiency $\eta_{\mathrm{SPC-IrR}}$ of 0.1688 bits per 4-QAM symbol (code rate $R_c = 0.0424$) by using EBSA. The parameters related to SPC-IrR, DACC, and MM are presented in the box in the figure. With this very low code rate, because of the area property, the area under the decoder curve is very small, which means that the decoder EXIT curve exhibits a "reverse-L" shape, and so is the demapper's EXIT curve. Because they are closely matched, near-capacity performance, very sharp BER threshold and error-floor removal (or reduction to a value range below $10^{-6} - 10^{-5}$ of BER) can be expected with the designed very low-rate code. Note that IDMA-SUD uses the code parameters and labeling pattern shown in Fig. 3.3.

3.3.3 Performance Evaluation of IDMA-SUD

BICM-ID-based IDMA-SUD does not require soft interference cancellation, and it only performs demapping and decoding, user-by-user, independently, without providing any *a priori* information to help the other users. Therefore, with IDMA-SUD, the BER performance versus SINR, defined by (3.9), is not affected by the number of the users, if the total user number K and the noise variance σ_n^2 are fixed. Fig. 3.4 plots BER performance of the proposed BICM-ID-based IDMA-SUD for $K = 6$, shown by "$\circ$". The BER threshold is very sharp, and no error floor can be observed (or invisible within the BER value range shown in the figure). It is found that the threshold SINR is around -8.69 dB, which is exactly consistent with the EXIT chart shown in Fig. 3.3, and this observation is independent of the number of the simultaneous users. The consistency between Figs. 3.3 and 3.4 indicates that it is reasonable to approximate the composite signal composed of the simultaneous users' signals plus Gaussian noise by equivalent Gaussian noise having the same power, at least, in a low enough SINR range.

3.4 Multiuser Detection

In Multiuser Detection (MUD), soft replica of each user's signal is subtracted from the received composite signal, of which process is referred to as soft cancellation. The outer iteration shown in Fig. 3.2 is now activated which indicates the outer iteration is included in MUD.

3.4.1 Detection Scheme of IDMA-MUD

In MUD, the received signal is expressed by (3.4)–(3.6), in the same way as in SUD. However, since the interference from the other users are eliminated by performing soft successive interference cancellation (SSIC) at the receiver side, the mean and the variance of the soft symbol, $\mathbb{E}[|x_{k,m}|]$ and $\sigma^2_{k,x,m}$, respectively, are updated every time the soft symbol is subtracted from the received composite signal, as shown in (16) and (17). The outer iteration is activated when no relevant gain in mutual information is achieved after several inner iterations alone.

The mean and the variance of the k-th user's soft symbol at the timing index m are updated by using

$$\mathbb{E}[|\hat{x}_{k,m}|] = \sum_{x_{k,m}\in S} x_{k,m} \prod_{\varpi=1}^{\ell} P(b_{k,\varpi} = \mp 1), \tag{3.11}$$

$$\sigma^2_{k,x,m} = 1 - \mathbb{E}[|\hat{x}_{k,m}|]^2 \tag{3.12}$$

with

$$P(b_{k,\varpi} = W) = \frac{e^{-b_{k,\varpi}\hat{L}_{k,p}}}{1 + e^{-\hat{L}_{k,p}}}, \tag{3.13}$$

where $W \in \{0, 1\}$ and ϖ is bit index of EM label. S is a set of constellation points. $\hat{L}_{k,p}$ denotes the *a posteriori* LLR fed back via the outer iteration to generate the soft symbol replica, $\hat{x}_{k,m} \equiv \mathbb{E}[|x_{k,m}|]$, defined as

$$\hat{L}_{k,p} = L_{k,a,dec,j} + L_{k,e,dec,j} + L_{k,p,dacc,j} \tag{3.14}$$

Obviously, before the first outer iteration is activated, the mean and the variance are

initialized, respectively, as

$$\mathbb{E}[|\hat{x}_{k,m}|] = 0, \tag{3.15}$$

$$\sigma^2_{k,x,m} = 1. \tag{3.16}$$

The soft interference cancellation can be expressed as

$$\hat{r}^t_m = r_m - \mathbb{E}[|\zeta^t_{k,m}|], \tag{3.17}$$

where

$$\mathbb{E}[|\zeta^t_{k,m}|] = \sum_{g=1}^{K} \sqrt{P_g} \cdot \mathbb{E}[|x^{t-1}_{g,m}|] - \sqrt{P_k} \cdot \mathbb{E}[|x^{t-1}_{k,m}|], \tag{3.18}$$

with t being the outer iteration index for each m-th transmission block. Then, the variance of the equivalent noise experienced by the k-th user after the soft cancellation via the outer iteration is given by

$$\hat{\sigma}^{t\ 2}_{k,\zeta,m} = \sum_{g=1,g\neq k}^{K} P_g \cdot \sigma^{t-1\ 2}_{g,x,m} + \sigma^2_n. \tag{3.19}$$

Thus, the equation for demapping, originally given by (3.8), can be rewritten for MUD as

$$L_{k,e,dem}[b_{k,d}] = \ln \frac{\displaystyle\sum_{x_{k,m}\in S_0} e^{-\frac{|\hat{r}^t_m - x_{k,m}|^2}{\hat{\sigma}^{t\ 2}_{k,\zeta,m}}} \prod_{q=1,q\neq d}^{\ell} e^{-b_q(s)L_{k,a,dem}(b_q(s))}}{\displaystyle\sum_{x_{k,m}\in S_1} e^{-\frac{|\hat{r}^t_m - x_{k,m}|^2}{\hat{\sigma}^{t\ 2}_{k,\zeta,m}}} \prod_{q=1,q\neq d}^{\ell} e^{-b_q(s)L_{k,a,dem}(b_q(s))}}, \tag{3.20}$$

where $\hat{r}^t_m$ and $\hat{\sigma}^{t\ 2}_{k,\zeta,m}$ are updated every time the outer iteration is activated and are provided to the demapper, before $L_{k,e,dem}[b_{k,d}]$ is calculated according to (3.20). The demapping equations in (3.8) and (3.20) can be calculated efficiently in the log-domain using the Jacobi algorithm [33, 34].

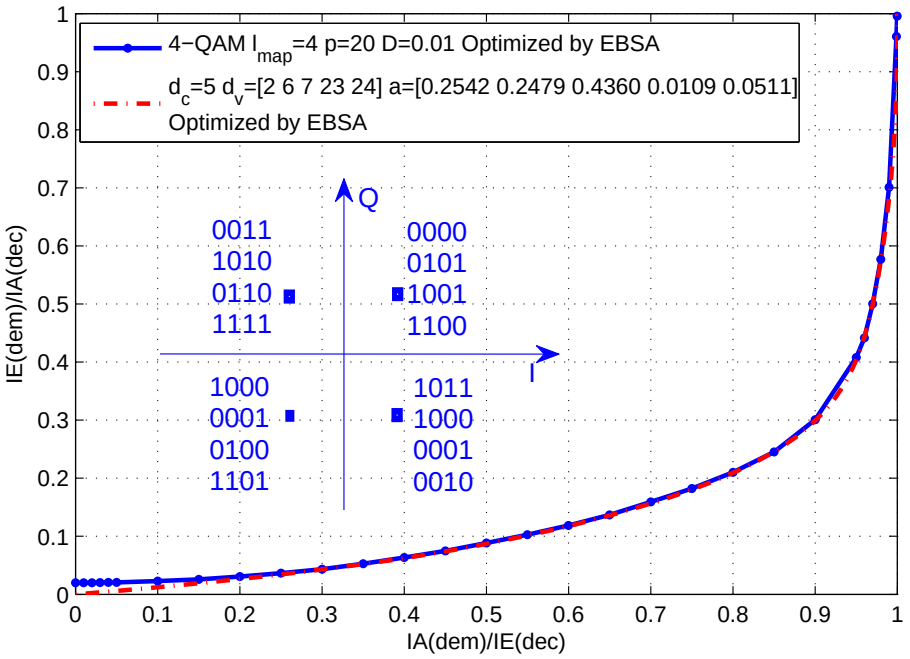

Figure 3.5: EXIT chart of IDMA-MUD technique at $SNR_k = -3.8$ dB, $k = 1, 2$ (Code rate $R_c = 0.1226$, Spectrum efficiency $\eta_{SPC-IrR} = 0.4879$ bits/4QAM-symbol).

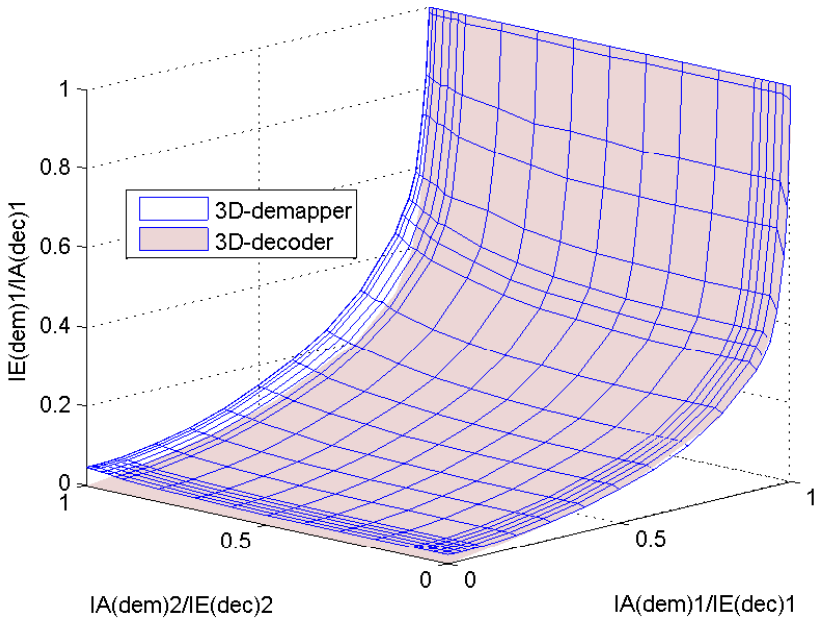

(a) Equal power allocation, $(P_1+P_2)/\sigma_n^2 = 2.21$ dB, $SNR_1 = SNR_2 = -0.8$ dB

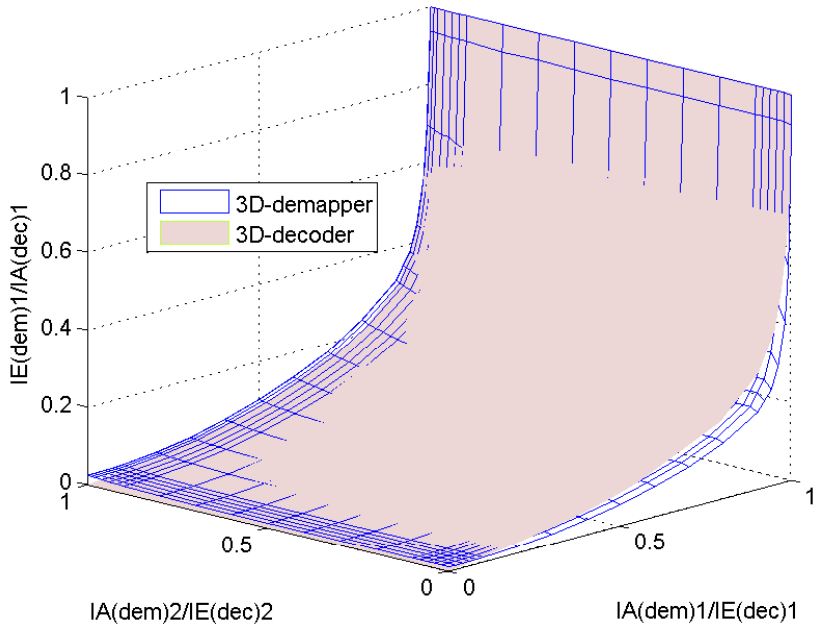

(b) Unequal power allocation, $(P_1 + P_2)/\sigma_n^2 = 0.63$ dB, $SNR_1 = -3.29$ dB, $SNR_2 = -1.62$ dB

Figure 3.6: 3D EXIT chart of IDMA-MUD technique.

3.4.2 EXIT Analysis of IDMA-MUD

As stated in Introduction, we assume the simplest two-user (K=2) IDMA MAC scenario to identify the convergence property and to focus on the impact of unequal power allocation. We first draw the demapper's EXIT curve by assuming that all the other users' signals are cancelled and we only consider one user. This assumption is reasonable because as described above, labeling patterns and coding parameters are determined by the EBSA algorithm so that two EXIT curves are very closely matched, and hence very sharp BER threshold can be expected. This means that if the labeling patterns and coding parameters are designed at a specified SNR value, SSIC can gradually but finally completely eliminate the other users' signals, without having to involve any statistical signal processing-based interference cancellation, as opposed to [9]. The EXIT curve obtained by using EBSA is presented in Fig. 3.5 for $SNR_k = -3.8$ dB. Since the simultaneous users provide the LLR feedback to each other, three-dimensional (3D) EXIT curves are used to visualize the convergence property.

Equal Power Allocation

Assume that the powers allocated to all users are equal, of which scenario is the same as the power allocation in SUD. A 3D EXIT chart is presented in Fig. 3.6(a) for $SNR_1 = SNR_2 = -0.8$ dB. It is found that the demapper and decoder planes are very close to each other, with a small gap near the (0.0, 0.0, 0.0) mutual information point. Hence, the LLR exchange can start. The tunnel opens in the most of the areas of the planes, and with the help of SSIC, the gap between the two planes becomes larger, and hence the trajectory is expected to directly reach a point very close to the (1.0, 1.0, 1.0) mutual information point. This will be confirmed in section 3.4.3.

Unequal Power Allocation

Assume that the powers allocated to different users are unequal but the total power P_{total} is kept constant. In this chapter, $P_{total} = 2.0$, for all the scenarios tested with two-user IDMA-MUD, and the noise variance is changed accordingly in this case. Fig. 3.6(b) presents the 3D EXIT chart in an unequal power allocation scenario where the ratio $P_1/P_2 = 0.68$, $SNR_1 = -3.29$ dB and $SNR_2 = -1.62$ dB. It is found that the two planes intersect at the most of the middle part where the decoder's EXIT plane is obviously above the demapper's. However, there still remains a gap, through which the trajectory is expected to go through and reach a point very close to the (1.0, 1.0, 1.0) mutual

information point. It should be noticed that for the both users, the SNR value is less than -0.8 dB, which is the case of equal power allocation, tested in the equal power allocation's case described above. This makes significant impact on the MAC region to be analysed in section 3.5.

3.4.3 Performance Evaluations of IDMA-MUD

The significant contribution of the research on BICM-ID-based IDMA over AWGN channels is the impact analysis of equal and unequal power allocation on MUD convergence property, also by using the multi-dimensional EXIT chart. Note again that since we assume only the simplest two-user IDMA in single-path AWGN channels, power allocation is intuitively equivalent in meaning to each user's transmit signal power. It is shown that with unequal power allocation, smaller total received SNR is required to achieve the BER threshold than with the equal power allocation. This result is consistent to [35].

With the proposed BICM-ID-based IDMA technique, excellent BER performance versus SINR can be achieved with SUD. However, when the number of users increases, BER versus each user's SINR, defined by (3.9), degrades due to the multiple access interference from the other simultaneous users. Therefore, to achieve better performance, a technique to reduce or to ultimately eliminate the interference, such as SSIC, is needed. Again, the simplest two-user scenario is assumed, and this sub-section investigates the BER performance of user 1 with the SSIC IDMA-MUD without loss of generality. The trajectory indicating the mutual information exchange obtained through chain simulation is also presented.

Performance of Equal Power Allocation

Fig. 3.8 presents 3D EXIT chart and the trajectory of the proposed BICM-ID-based IDMA-MUD for $K = 2$ users, respectively, where the $SINR_1 = SINR_2 = -3.43$ dB ($SNR_1 = SNR_2 = -0.8$ dB and $(P_1 + P_2)/\sigma^2 = 2.21$ dB). The BER performance in this scenario is shown by "□" in Fig. 3.7. With our proposed technique, the BER threshold is very sharp and no error-floor is visible in the BER range. Due to the exactly matched EXIT curves combined with the soft cancellation technique, very near-capacity performance, only 0.52 dB away from the limit, can be achieved. It is found that the trajectory directly goes through the middle part between the two planes, and reaches a point very close to the (1.0, 1.0, 1.0) mutual information point, as expected in sub-section 3.4.2.

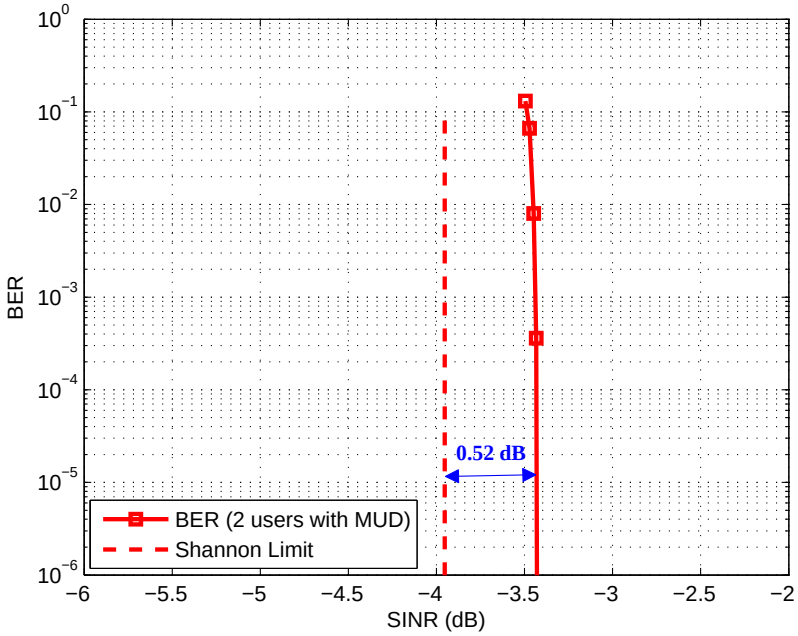

Figure 3.7: The BER performance of IDMA-MUD.

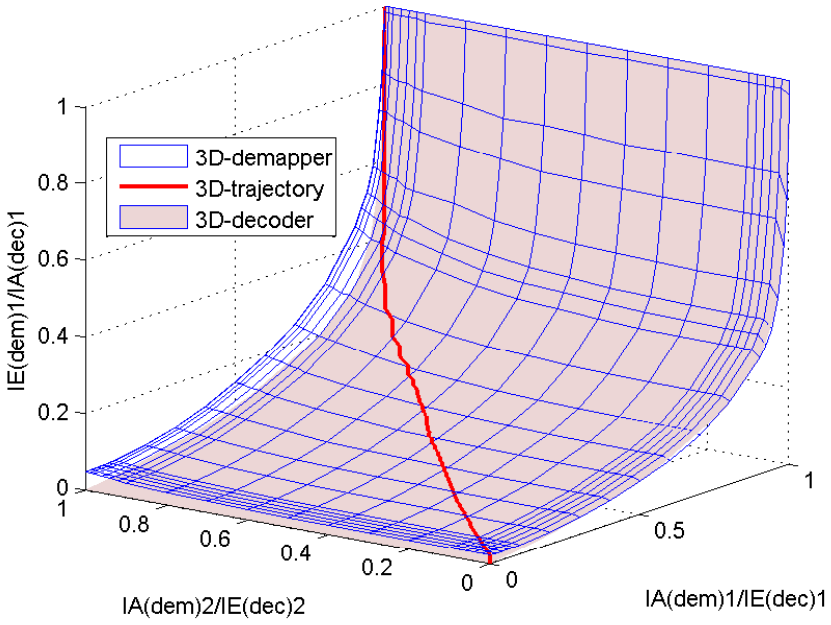

Figure 3.8: The trajectory of IDMA-MUD with equal power allocation, $SNR_1 = SNR_2 = -0.8$ dB.

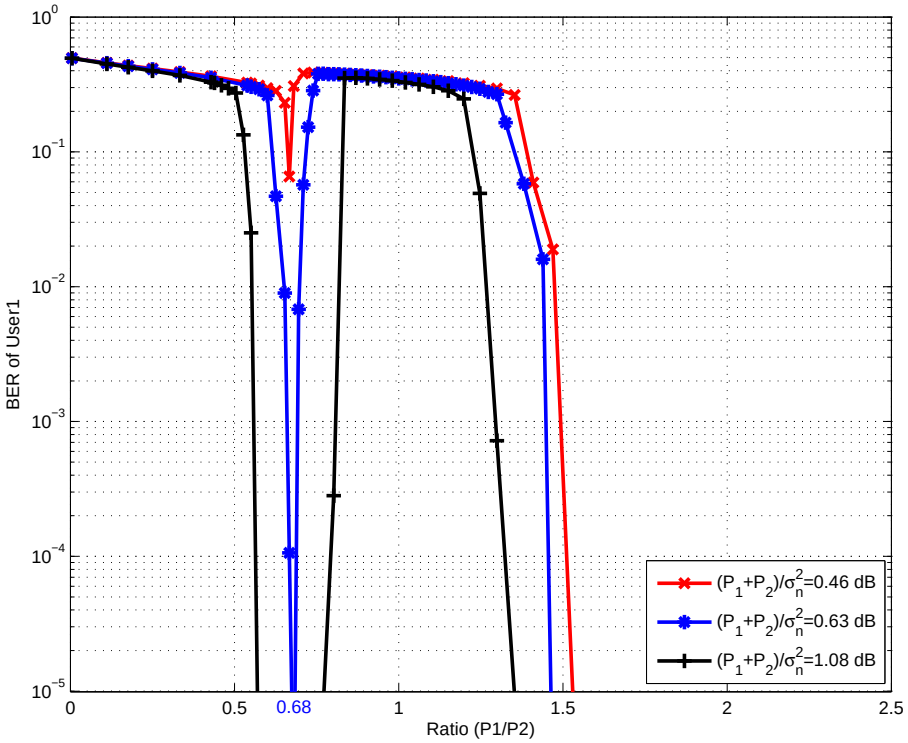

Figure 3.9: BER performance of IDMA-MUD for $K = 2$ users with unequal power allocation.

Performance of Unequal Power Allocation

Assume that the total power is fixed as $(P_1 + P_2) = 2.0$ such that $(P_1 + P_2)/\sigma_n^2 = 1.08$ dB, while changing the ratio of P_1/P_2. The results of the simulations conducted to evaluate the BER performance with unequal power allocation, are plotted in Fig. 3.9. It is found from the figure that the BER curve shown by "+" for user 1 first decreases very sharply as the ratio P_1/P_2 increases, and it becomes lower than 10^{-5} between $P_1/P_2 = 0.58$ and $P_1/P_2 = 0.75$, and then it suddenly increases to a value larger than 10^{-1}, when $P_1/P_2 \cong 1.0$. Then, after that, it sharply decreases again when $P_1/P_2 \geq 1.3$. When the $(P_1 + P_2)/\sigma_n^2$ is decreased to 0.63 dB, the BER curve shown in "*" has almost the same tendency, still the rapid decrease in BER can be found around $P_1/P_2 = 0.68$, when the ratio $P_1/P_2 < 1.0$. However, the BER curve shown in "×" is for $(P_1 + P_2)/\sigma_n^2 = 0.46$ dB where the same labeling pattern and code parameters, including the switching and mixing ratios, p and D, respectively, are used as in the case of $(P_1 + P_2)/\sigma_n^2 = 1.08$ dB. A similar tendency can be observed but the rapid decrease in BER can not be observed, when the ratio $P_1/P_2 < 1.0$. Hence, $(P_1 + P_2)/\sigma_n^2 = 0.63$ dB is identified as the limit case with this code parameters set and labeling pattern. In the following part, we focus on the limit case so as to make comparison among several unequal power allocation cases as well as with a counterpart technique, shown in section 3.5.

The trajectories representing the mutual information exchange are investigated at the ratios of $P_1/P_2 = \{1.0, 0.6, 0.68\}$ with $(P_1 + P_2)/\sigma_n^2 = 0.63$ dB. Fig. 3.10(a) shows the trajectory for $P_1/P_2 = 1.0$ in the 3D EXIT chart. It is found that although there is a gap between the planes of demapper and decoder, the trajectory is stuck at a relatively low mutual information point. This is because with $P_1/P_2 = 1.0$, $SNR_1 = SNR_2 = -2.38$ dB and $(P_1 + P_2)/\sigma_n^2 = 0.63$ dB, the two planes are so close to each other around the (0.0, 0.0, 0.0) mutual information point and hence the trajectory can not go through the tunnel. Fig. 3.10(b) shows the trajectory for $P_1/P_2 = 0.6$ ($SNR_1 = -3.62$ dB, $SNR_2 = -1.4$ dB and $(P_1 + P_2)/\sigma_n^2 = 0.63$ dB). It is found that the two planes intersect in the most of the middle part of the 3D EXIT chart, however, there still exists a small gap on the left side, and the tunnel is open until the *extrinsic* mutual information of the demapper for user 1 is around 0.35 and hence the trajectory can reach the point (demapper's *extrinsic* mutual information = 0.35 for the $user1$). Furthermore, it is found from the trajectory that for user 2, decoder's *extrinsic* mutual information reaches very close to 1.0. This means that user 2 can be nearly fully detected without errors while user 1 can not be fully detected. Fig. 3.10(c) presents the trajectory for $P_1/P_2 = 0.68$ ($SNR_1 = -3.29$ dB, $SNR_2 = -1.62$ dB and $(P_1 + P_2)/\sigma_n^2 = 0.63$ dB). It is found that the two planes intersect in the most

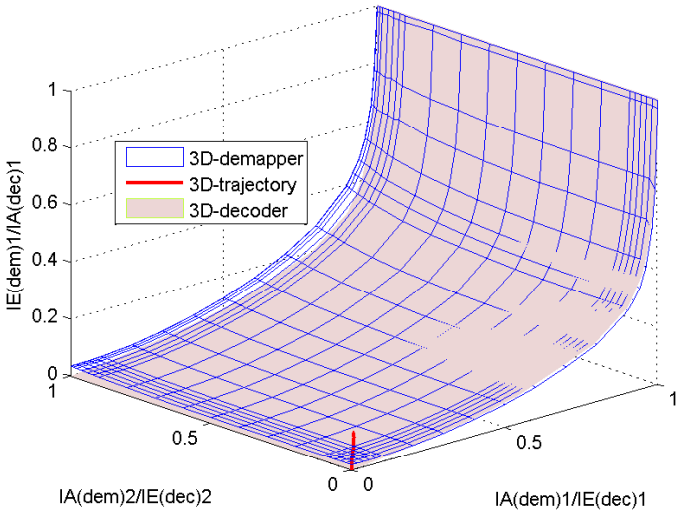

(a) $P_1/P_2 = 1$, $(P_1 + P_2)/\sigma_n^2 = 0.63$ dB

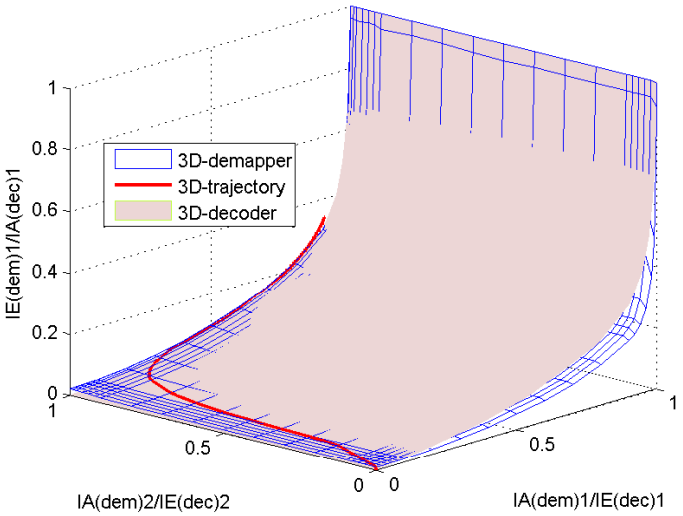

(b) $P_1/P_2 = 0.6$, $(P_1 + P_2)/\sigma_n^2 = 0.63$ dB

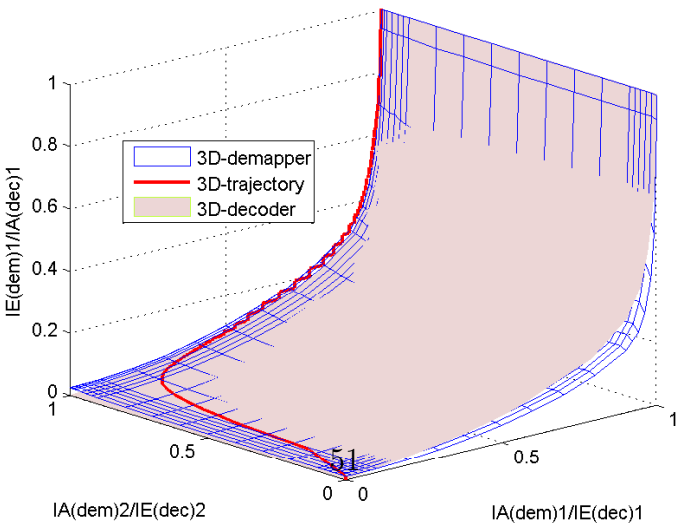

(c) $P_1/P_2 = 0.68$, $(P_1 + P_2)/\sigma_n^2 = 0.63$ dB

Figure 3.10: The trajectories of IDMA-MUD with unequal power allocation.

of the middle part of the 3D EXIT chart, but a gap still exists near the left edge of the two planes, and the tunnel opens until a point very close to the (1.0, 1.0, 1.0) mutual information point. The trajectory can sneak through the gap between the two planes, and reach the point very close to (1.0, 1.0, 1.0) mutual information point, which also means both the two users can be fully detected, even with smaller $(P_1 + P_2)/\sigma_n^2$ value (0.63 dB), compared with equal power allocation case, whose $(P_1 + P_2)/\sigma_n^2$ value is 2.21 dB.

3.5 MAC Rate Region Analysis

It is of our great interest to make the MAC rate region comparison between equal and unequal power allocation cases, as well as between our proposed and [9]'s proposed technique. The scenario with $K = 2$ is considered for the both equal and unequal power allocation cases. To calculate the MAC rate region, we assume that all the users use Gaussian codebook. The points in the MAC rate region A_1 and A_2, as defined in Fig. 3.11, are given by

$$A_1 = C\left(\frac{P_1}{\sigma_n^2}\right), \tag{3.21}$$

$$A_2 = C\left(\frac{P_1}{P_2 + \sigma_n^2}\right), \tag{3.22}$$

with $C(x) = \log_2(1 + x)$.

B_1 and B_2 are defined in the same way as the points A_1 and A_2 by replacing the user index 1 by 2. Moreover, since we are assuming $P_1 = P_2 = 1.0$ for the case of equal power allocation, and $P_1 + P_2 = 2.0$, while changing σ_n^2 and P_1/P_2 values for the unequal power allocation case.

From Fig. 3.7 we first determined the $SINR_k$ value required to achieve 10^{-6} BER for $P_1/P_2 = 1.0$ and $(P_1 + P_2)/\sigma_n^2 = 2.21$ dB, then, all the values of the argument of $C(x)$, which is needed to calculate (3.21)–(3.22), can be determined for equal power allocation case. For the unequal power allocation case, those values were directly obtained from $P_1/P_2 = 0.68$, $(P_1 + P_2)/\sigma_n^2 = 0.63$ dB and $P_1 + P_2 = 2.0$ (Recall that the rapid decrease of BER happens at $P_1/P_2 = 0.68$, as shown in Fig. 3.9). Fig. 3.11 shows the MAC rate regions (or MAC-pentagon) with the equal and unequal power allocation cases. It is found that the MAC rate region with unequal power allocation is smaller than that with equal power allocation. However, the achieved spectrum efficiency of two cases are the same, i.e, $R_1 = R_2 = \eta_{\text{SPC-IrR}} = 0.4879$ bits per 4-QAM symbol, which is shown

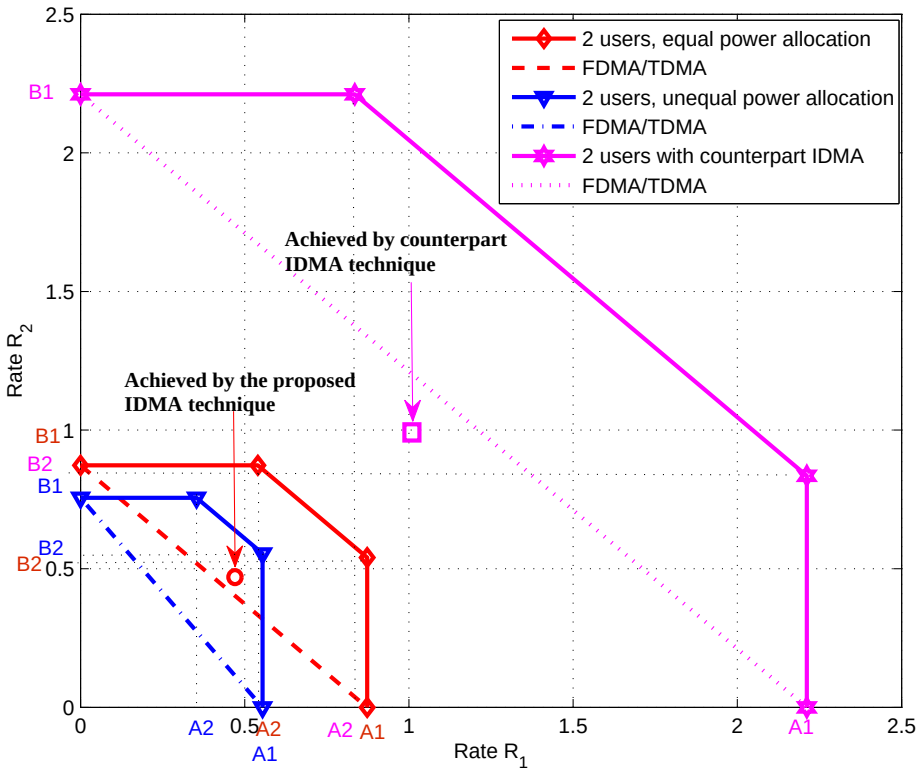

Figure 3.11: Gaussian multiple access channels for $K = 2$ users (the comparison between our proposed IDMA technique (with equal and unequal power allocation cases) and IDMA counterpart technique proposed by [9]), equal power allocation: $SNR_1 = SNR_2 = -0.8$ dB, unequal power allocation: $SNR_1 = -3.29$ dB, $SNR_2 = -1.62$ dB.

in Fig. 3.11 by "$\circ$". This confirms that unequal power allocation can achieve the same spectrum efficiency with smaller SNR values.

The dotted line connecting A_i and B_i, $i = \{1, 2\}$, corresponds to two-user orthogonal signalling such as frequency or time division multiple access (FDMA or TDMA). It is found that with both the equal and unequal power allocation cases, the rate-pair plot is above the FDMA/TDMA line, and with the unequal power allocation, the plot is closer to the theoretical MAC rate region.

The upper bound of the sum-rate $R_1 + R_2$ is given by

$$R_1 + R_2 \leq C\left(\frac{P_1 + P_2}{\sigma_n^2}\right) \tag{3.23}$$

It is found from Fig. 3.11 that the MAC rate region with unequal power allocation is smaller than that with equal power allocation, and obviously, with the unequal power allocation, the MAC region is not symmetric. With the equal power allocation ($SNR_1 = SNR_2 = -0.8$ dB), the sum-rate bound B_{equal} is 1.41, while with unequal power allocation ($SNR_1 = -3.29$ dB and $SNR_2 = -1.62$ dB), the sum-rate bound $B_{unequal}$ is 1.1. Therefore, we can conclude that the achieved sum-rate $R_1+R_2 = 2\times0.4879$, and $R_1+R_2<$ $B_{unequal}$ ($SNR_1 = -3.29$ dB and $SNR_2 = -1.62$ dB)$<B_{equal}$ ($SNR_1 = SNR_2 = -0.8$ dB). It can be concluded that to achieve the same spectrum efficiency ($\eta_{\mathrm{SPC-IrR}} = 0.4879$), unequal power allocation requires smaller $SNRs$ values for each user.

It is interesting to make comparison of the achieved rate pair and the MAC rate region between our proposed and [9]'s proposed techniques. Since [9] assumes an 8 user IDMA scenario, we converted the rate pair and the MAC region to the two-user case by the following method: first of all, we identified the SNR value, required to achieve 10^{-6} BER from Fig. 3 in [9]. Since, in [9], all users use the same code, which achieves 0.2550 bits per 4-QAM symbol, and the same power is allocated to them, A1 point in Fig. 3.11 can be calculated by assuming that 6 out of 8 users are totally cancelled, and A2 by assuming that 6 out of 8 users are equivalent to noise. The point B1 and B2 can also be calculated in the same way.

Since spectrum efficiency of the system proposed in [9] is 0.2550 bits per 4-QAM symbol for all the 8 users, it is equivalent to each user's spectrum efficiency of 1.02 bits per 4-QAM symbol in two-user case, assuming a Gaussian codebook. The calculated MAC region and the rate pair (indicated by "$\square$") obtained by converting from 8 user IDMA to two-user IDMA are also shown in Fig. 3.11. It is found that surprisingly the achieved rate pair with [9]'s technique is lower than the FDMA/TDMA line with a Gaussian codebook.

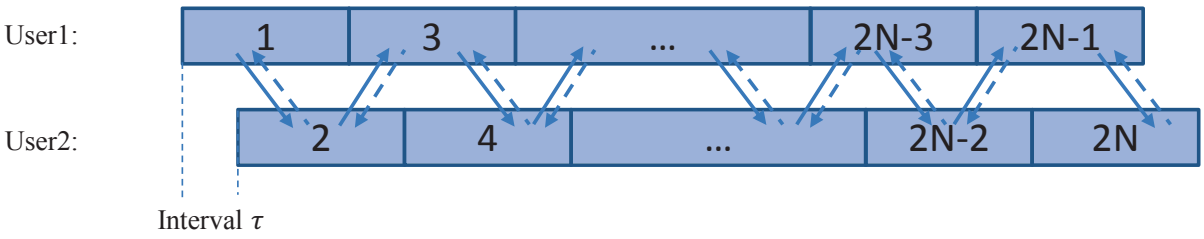

Figure 3.12: Asynchronous frame timing.

Obviously, this is because the code used in [9] (a convolutional code combined with a low rate repetition code) can achieve neither near-capacity performance nor very sharp BER threshold.

3.6 Asynchronous IDMA

The scenario assumption made for the BICM-ID-based IDMA algorithm design and performance evaluation, described above, has assumed the perfect synchronism among the different users. Since IDMA uses interleavers to distinguish different users. Interleaver also plays an important role in the iterative detection. This observation indicates that IDMA detects the signals of each user by considering the other users' signals as being equivalent to noise, regardless of the relationship among the different users as in the soft cancelation process. For example, in SUD, when concentrating on one user, the other users' signals are equivalent to noise. So does in the inner iteration of MUD. Hence, it is supposed that proposed IDMA is robust against the frame-asynchronism.

In order to study this issue, we construct an asynchronous BICM-ID-based IDMA system model by adding certain transmission delay for each user. As shown in Fig. 3.12, for simplicity, we consider the case where there are 2 users in the transmitter part. The transmission delay, between 2 different users's transmitted siganls, is defined as the interval τ. Thus, in the receiver part, the received signal is the mixture of two asynchronous users' signals with a delay interval τ plus noise. Here, we assume that the start and end point of each frame is known.

In Fig. 3.12, since each frame of user1 is not synchronized with each frame of user2, for example the first frame of user2 is overlaping with the first and second frames of user1. Performing the MUD technique described above neither between the first frame of user2 and the first frame of user1 nor between the first frame of user2 and the second frame of user1 can fully eliminate the interference from the other user. To detect the asynchronous

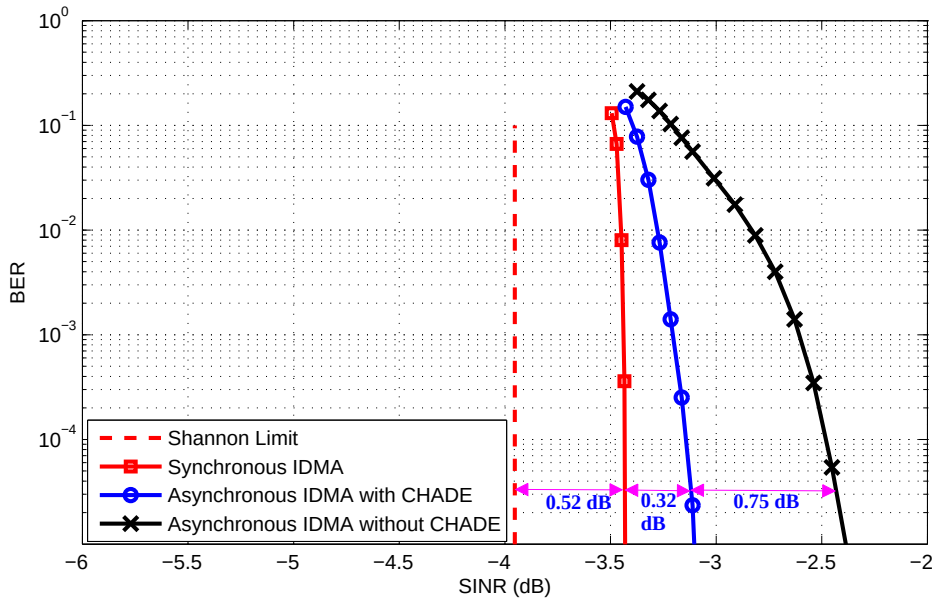

Figure 3.13: The comparison of the BER performance between synchronous and asynchronous IDMA.

received frames as shown in Fig. 3.12, we propose a chained detection (CHADE) technique, with which multiple frames are jointly detected by performing the iterative MUD on the frame by frame basis with the order indicated in each frame, $1, 2, ..., 2N-1, 2N$, as shown in Fig. 3.12: start from the first frame of user1, then the first frame of user2, ..., until the last frame of user1 and the last frame of user2, as illustrated with the solid arrows. Then, soft cancelation applies to the each signal's overlapping parts. After the soft cancellation, the frame-wise detection is again performed but in backward direction, i.e. $2N, 2N-1, ..., 2, 1$, as illustrated with the dashed arrows. This forward and backward recursion is repeated until all the frames are detected.

The computer simulations are conducted to evaluate the BER performance of the constructed asynchronous IDMA system with delay interval, τ symbol-durations (τ is a random integer that uniformly distributes in the range 1 to 100). The code parameters and labeling pattern are the same as shown in Fig. 3.5 with the transmitted symbol length 20000. The simulation results are presented in Fig. 3.13, where the curve plotted with "$\circ$" is the BER performance of the asynchronous IDMA with performing the proposed CHADE technique and the curve shown with "$\times$" is the BER performance of the asynchronous IDMA without performing the CHADE technique. It can be observed that the BER performance with CHADE technique outperforms that without CHADE technique, which indicates that with the CHADE technique, the BER performance has been improved 0.75 dB. Then, the comparison is made between the BER performance of the asynchronous IDMA with performing the proposed CHADE technique and the BER performance of the synchronous IDMA described in Fig. 3.7. It is found that the BER performance of the asynchronous IDMA proposed with performing the proposed CHADE technique is very close to the synchronous case, only 0.32 dB gap between the two cases. This comparison shows that the proposed IDMA system is robust against the frame-asynchronism.

3.7 Summary

In this chapter, the main objective has been to propose a new BICM-ID-based IDMA system and to evaluate its performance.

First of all, the IDMA principle was introduced which was followed by the system design of proposed IDMA system based on BICM-ID structure, of which the SUD and MUD schemes are detailed. The EXIT chart analysis and the performance evaluations of each scheme were also presented. It was shown that the near-capacity performance can

be achieved by both of the schemes.

We then analyzed the impact of the power allocation on the convergence and the MAC rate region. The 3D EXIT and trajectory as well as the MAC rate region analysis clearly demonstrated the impact of power allocation on the performance of the system that the unequal power allocation can achieve the same spectrum efficiency with smaller SNR.

Finally, a CHADE technique was proposed for the asynchronous IDMA system. Robustness of the proposed IDMA system, with repeated CHADE technique against frame-asynchronism, was proven through computer simulations where certain transmission delay was added for each user. The simulation result indicated that the proposed IDMA technique is robust against the frame-asynchronism.

Chapter 4

Joint Turbo Equalization and BICM-ID-based IDMA

In **Chapter 3**, we proposed BICM-ID-based IDMA system with SUD and MUD over AWGN channels, where the convergence property and rate region were also analyzed. In this chapter, the proposed BICM-ID-based IDMA system is extended to frequency selective fading channels by combining with a FD-SC-MMSE turbo equalization so that both the MAI and ISI can be eliminated. Moreover, in order to improve the efficiency of the system, a DO technique is introduced.

First of all, the new system model, with the DO technique and the FD-SC-MMSE equalization, is presented. Then, the scheme of joint turbo equalization and IDMA signal detection, which makes the BICM-ID-based IDMA system work well in frequency selective fading channels, is detailed. After that, the principle of DO is explained, which is followed by the performance evaluation of the proposed system in frequency selective fading channels.

4.1 System Model

The system model investigated in this chapter is based on the BICM-ID-based IDMA system described in **Chapter 3**. Since in **Chapter 3**, we found that unequal power allocation achieve better performance than equal power allocation, which invokes the idea that in fading environments, DO plays a very important role in achieving excellent performance. Motivated by this idea, this detection introduces a joint turbo equalization and IDMA signal detection scheme as well as a DO technique [36].

A schematic diagram of the BICM-ID-based IDMA system is depicted in Fig. 4.1. Each

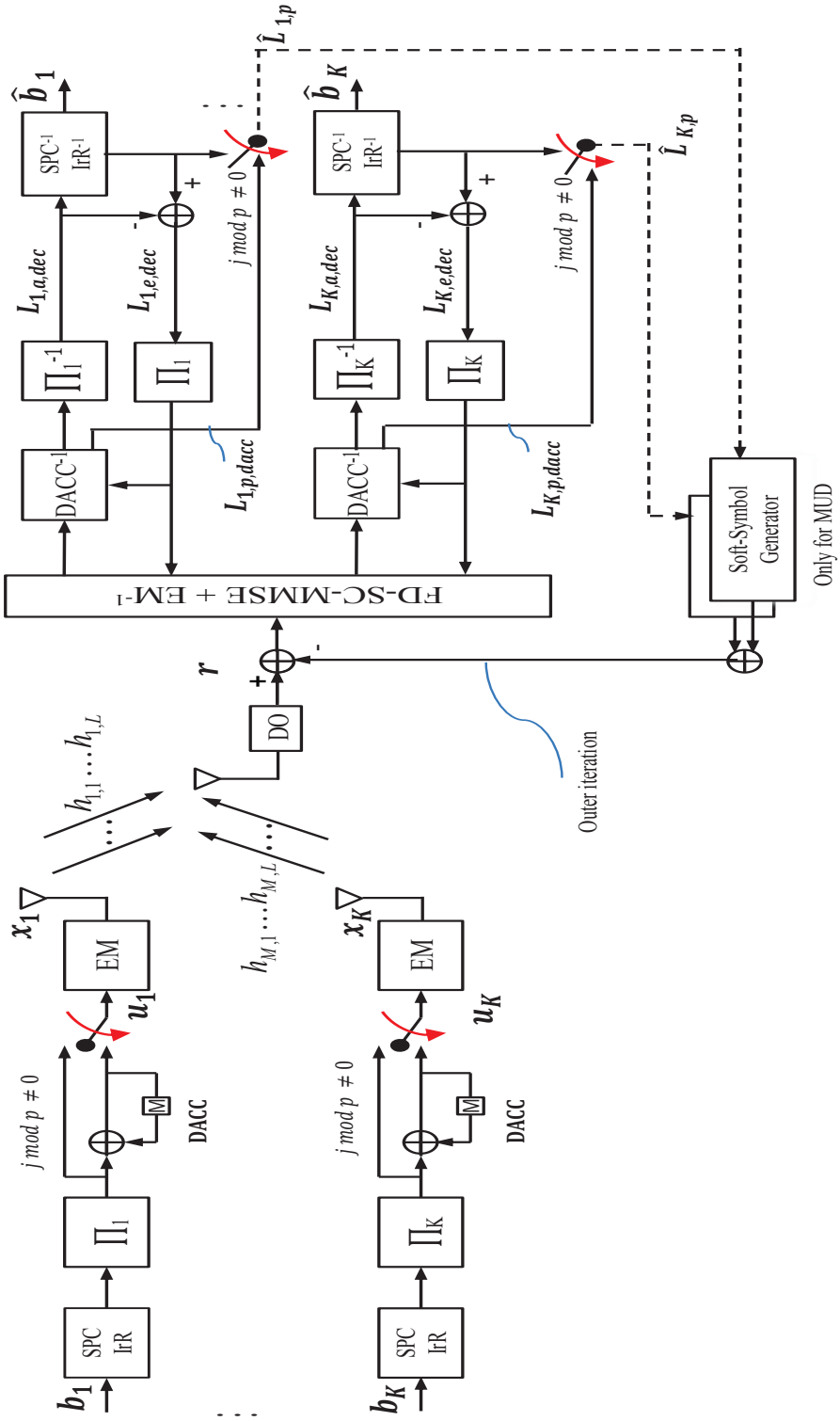

Figure 4.1: A schematic diagram for the proposed joint turbo equalization and BICM-ID-based IDMA system.

user uses the same BICM transmission chain, where the binary bit information sequence $\mathbf{b}_k$ of k-th user is first encoded by the SPC-IrR encoder with the parameters d_c, d_v, a, and then bit-interleaved by a random interleaver Π_k. After that, in DACC, the coded interleaved bit sequence is doped-accumulated [11] with a doping ratio p [27] and output a new bits sequence $\mathbf{u}_k$. The output binary sequence $\mathbf{u}_k$ is serial-to-parallel converted, and mapped on to a 4-QAM signal point, in part, according to the labeling pattern for EM determined by EBSA, and in part, according to the non-Gray labeling pattern [10] to generate transmission symbols $\mathbf{x}_k$, with modulation mixing ratio D. The parameters of the codes and labeling pattern are shown in the EXIT chart in section 4.4.

The modulated symbol sequence $\mathbf{x}_k$ is then transmitted over frequency selective fading channels. l denotes the channel multipath index, $l \in \{1, \cdots, L\}$ with L being the number of the paths. The fading channel gains are assumed to be constant during one block interval, but vary block-by-block. Let $\mathbf{H}_k$ denote the equivalent block-wise representation of the channel matrix for k-th user. Cyclic prefix (CP) transmission is also assumed in this chapter. When CP is appended at the transmitter side and eliminated at the receiver side, the equivalent channel matrix $\mathbf{H}_k$ becomes circulant matrix $\mathbf{H}_k^c$ in multipath channels. The circulant matrix $\mathbf{H}_k^c$ for the k-th user is shown by

$$\mathbf{H}_k^c = \begin{bmatrix} h_{k,1} & 0 & \cdots & h_{k,L} & \cdots & h_{k,2} \\ h_{k,2} & h_{k,1} & \cdots & 0 & \cdots & h_{k,3} \\ \vdots & \vdots & \vdots & \vdots & \vdots & \vdots \\ h_{k,L} & h_{k,L-1} & \cdots & 0 & \cdots & h_{k,L} \\ 0 & h_{k,L} & \cdots & 0 & \cdots & 0 \\ \vdots & \vdots & \vdots & \vdots & \vdots & \vdots \\ 0 & 0 & \cdots & h_{k,L-1} & \cdots & h_{k,1} \end{bmatrix}, \tag{4.1}$$

where $\mathbf{H}_k^c \in \mathbb{C}^{(M+L-1)\times M}$ and $h_{k,l}$ is the complex channel gain of l-th path with the channel of the k-th user.

Then, the equivalent frequency domain channel matrix Ξ can be obtained by utilizing the property of the circularity of matrix $\mathbf{H}_k^c$, expressed as

$$\Xi = \mathbf{F}^H \mathbf{H}_k^c \mathbf{F}, \tag{4.2}$$

where the Fourier matrix $\mathbf{F} \in \mathbb{C}^{N\times N}$ has each element defined as $\mathbf{F}_{i,j} = M^{-\frac{1}{2}} e^{-\jmath \frac{2\pi}{M}(i-1)(j-1)}, \jmath = \sqrt{-1}, i, j = 1, \cdots, M$, with M being the block length.

When the blocks of the symbol squences $\mathbf{x}_k$, $k = 1, ..., K$, are simultaneously transmit-

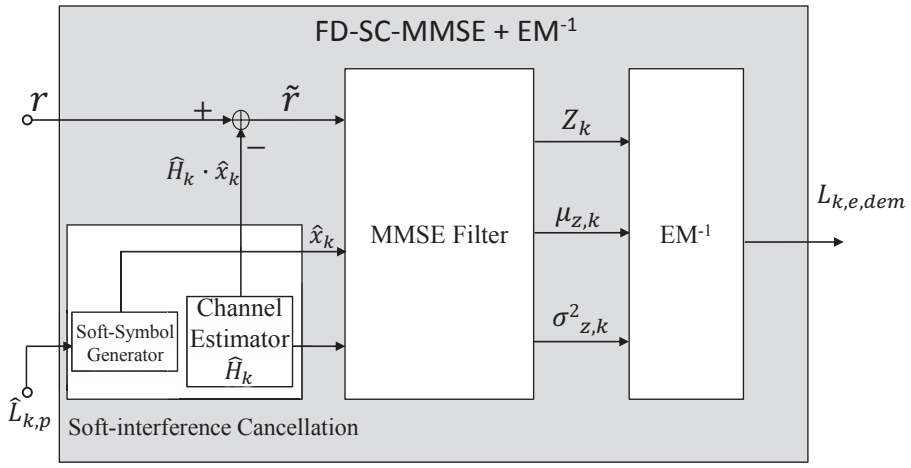

Figure 4.2: Joint turbo equalizer and EM demapper.

ted over their corresponding channels, the received signal $\mathbf{r}$ can be expressed as

$$\mathbf{r} = \sum_{k=1}^{K} \sqrt{P_k} \cdot \mathbf{H}_k^c \cdot \mathbf{x}_k + \mathbf{n}, \tag{4.3}$$

where P_k and $\mathbf{n}$ denote the power of the k-th user and the AWGN component with variance σ_n^2, respectively.

4.2 Joint Turbo Equalization and IDMA Signal Detection

In this chapter, we propose a joint frequency domain turbo equalization and IDMA signal detection technique based on the BICM-ID-based IDMA proposed in **Chapter 3**. FD-SC-MMSE turbo equalization is considered as a compelling technique to implement that well-performs equalization without requiring excessive computational complexity. The joint use of turbo equalization and IDMA signal detection makes the BICM-ID-based IDMA system possible in more practical, frequency selective fading channels. The structures and principles for DACC decoder and SPC-IrR channel decoder have been presented in detail in the previous chapters. The frequency domain algorithm of FD-SC-MMSE equalizer is provided in [37]. In this chapter, we derive the joint utilization of Turbo equalization and IDMA signal detection.

The joint turbo equalization and IDMA signal detection consists of a FD-SC-MMSE equalizer and SPC-IrR soft-in-soft-out channel decoders for each user. These are separated

by DACC decoding, deinterleaving and interleaving operations as illustrated in Fig. 4.1. There are two types of iterations, one is inner iteration which is performed between FD-SC-MMSE equalizer and SPC-IrR channel decoder for each user, the other one is outer iteration performed between different users. The outer iteration is activated once all users finish one round specific times inner iterations. A block diagram of joint FD-SC-MMSE equalizer and EM demapper is shown in Fig. 4.2. It should be noticed that we assume channel knowledge is perfectly known in the transmitter side. It means that the channel estimator $\hat{H}_k \equiv H_k$.

4.2.1 Soft-interference Cancelation

Since the interference from the other users can be eliminated by performing soft interference cancelation at the receiver side, the soft symbol and the variance of the soft symbol, $\hat{x}_{k,m}$ and $\sigma^2_{k,m}$, have to be updated every outer iteration.

The $\hat{x}_{k,m}$ and $\sigma^2_{k,m}$ at timing index m are updated by using

$$\hat{x}_{k,m} = \sum_{s \in S} s \prod_{\varpi=1}^{lmap} P(b_{k,\varpi} = \mp 1), \tag{4.4}$$

$$\sigma^2_{k,m} = 1 - |\hat{x}_{k,m}|^2, \tag{4.5}$$

with

$$P(b_{k,\varpi} = W) = \frac{e^{-b_{k,\varpi}\hat{L}_{p,k}}}{1 + e^{-\hat{L}_{p,k}}}, \tag{4.6}$$

where $W \in \{0, 1\}$ and ϖ is the bit index in an EM label. The labeling length$lmap$ is the parameter of EM; with $lmap = 4$, one constellation point represents 4 labeling patterns. S is a set of constellation points. $\hat{L}_{k,p}$ denotes the *a posteriori* LLR fed back via the outer iteration to generate the soft symbol replica, defined as

$$\hat{L}_{k,p} = L_{k,a,dec} + L_{k,e,dec} + L_{k,p,dacc}. \tag{4.7}$$

Before the first outer iteration is activated, the value of $\hat{x}_k$ and σ^2_k are initialized as

$$\hat{x}_{k,m} = 0, \tag{4.8}$$

$$\sigma^2_{k,m} = 1. \tag{4.9}$$

The residual of the ISI $\tilde{\mathbf{r}}$ after soft interference cancelation are updated every outer iteration by using received composite signal $\mathbf{r}$ to substract all the users' soft symbols, as

$$\tilde{\mathbf{r}} = \mathbf{r} - \sum_{k=1}^{K} \sqrt{P_k} \cdot \mathbf{H}_k^c \cdot \quad \hat{\mathbf{x}}_k, \tag{4.10}$$

where

$$\hat{\mathbf{x}}_k = [\hat{x}_{k,1}, \hat{x}_{k,2}, ..., \hat{x}_{k,m}, ..., \hat{x}_{k,M}] \tag{4.11}$$

M is the length of soft symbol.

The corresponding variance of ISI, $\hat{\sigma}_m^2$, after the soft cancelation via the outer iteration is given by

$$\hat{\sigma}_m^2 = \sum_{g \neq m, g=1}^{M} E_g \cdot P_g \cdot \sigma_g^2 + \sigma_n^2. \tag{4.12}$$

with total channel power of the g-th user being

$$E_g = \sum_{l=1}^{L} |h_{g,l}|^2. \tag{4.13}$$

4.2.2 MMSE Filter

After soft cancelation, the ISI residual $\tilde{\mathbf{r}}$ and the perfect channel state $\hat{H}_k$ are forwarded to MMSE filter, as shown in Fig. 4.2. In this frequency domain equalizer, the output vector of the MMSE estimates of the transmitted symbols for the k-th user, can be expressed as

$$\mathbf{Z}_k = (1 + \bar{\gamma}_k \cdot \bar{\delta}_k)^{-1} \cdot [\bar{\gamma}_k \cdot \hat{\mathbf{x}}_k + \mathbf{F}^H \Psi_k \tilde{r}_k^f], \tag{4.14}$$

where the following definitions have been used

$$\bar{\gamma}_k = \frac{1}{M} tr[\Xi^{fH} (\Xi^f \Delta \Xi^{fH} + \hat{\sigma}_k^2 I_{NM})^{-1} \Xi^f], \tag{4.15}$$

$$\bar{\delta}_k = \frac{1}{M} \sum_{m=1}^{M} |\hat{\mathbf{x}}_k(m)|^2, \tag{4.16}$$

$$\Psi_k = \Xi^{fH} (\Xi^f \Delta \Xi^{fH} + \hat{\sigma}_k^2 I_{NM})^{-1}. \tag{4.17}$$

The Ξ and Δ are defined as

$$\Xi = \mathbf{F}\mathbf{H}_k^c\mathbf{F}, \tag{4.18}$$

$$\Delta = \mathbf{F}\Lambda\mathbf{F}^H \approx \frac{1}{M}tr\Lambda, \tag{4.19}$$

with $\Lambda = I_M - diag[|\hat{\mathbf{x}}_k|^2]$. Hence, the first and second moments of the MMSE filter output are expressed as

$$\mu_{z,k} = \bar{\gamma}_k(1+\bar{\gamma}_k\bar{\delta}_k)^{-1}, \tag{4.20}$$

$$\sigma_{z,k}^2 = \mu_{z,k}(1-\mu_{z,k}). \tag{4.21}$$

4.2.3 EM Demapper

Now, we can convert the MMSE filter outputs into the *extrinsic* LLR for the k-th user in EM demapper, and the output of EM demapper described in **Chapter 3** can be rewritten as

$$L_{k,e,dem}[b_{k,d}] = \ln \frac{\sum_{s\in S_0} e^{-\frac{|\mathbf{z}_k-\mu_{z,k}\cdot s|^2}{\hat{\sigma}_{z,k}^2}} \prod_{q=1,q\neq d}^{lmap} e^{-b_q(s)L_{k,a,dem}(b_q(s))}}{\sum_{s\in S_1} e^{-\frac{|\mathbf{z}_k-\mu_{z,k}\cdot s|^2}{\hat{\sigma}_{z,k}^2}} \prod_{q=1,q\neq d}^{lmap} e^{-b_q(s)L_{k,a,dem}(b_q(s))}}. \tag{4.22}$$

$\mathbf{Z}_k$, $\mu_{z,k}$ and $\sigma_{z,k}^2$ are updated every time the outer iteration is activated and they are provided to the demapper, before $L_{k,e,dem}[b_{k,d}]$ is calculated according to (4.22). After the demapping process, the output of the FD-SC-MMSE equalizer $\mathbf{L}_{k,e,dem}$ is forwarded to DACC decoder and the inner iteration for k-th user is activated.

4.3 Detection Ordering

The box indicated by Detection Ordering (DO) in Fig. 4.1 between antenna and FD-SC-MMSE equalizer determines the detection order of the users by comparing the channel gains E of each user. For the g-th user, E_g is shown in (4.13). The algorithm of DO is summarized in **Algorithm** 1.

The detection order $\mathbf{D}$ is determined by the DO box before the detector starts the

Input: **E** is a *set* containing each user's total channel power
$\mathbf{E} = \{E_1, E_2, ..., E_k, ..., E_K\}$ and the corresponding indexes are in *set*
$\mathbf{K} = \{1, 2, ..., k, ..., K\}$
Output: Detection order *set* **D**
$\mathbf{D} = \varnothing$;
for $j = 1; j \leq K; j++$ **do**
  T=*set* **K***set* **D**;
  while $\mathbf{T} \neq \varnothing$ **do**
    $\mathbf{D}(j) = \underset{\kappa \in \mathbf{T}}{argMAX}(E_\kappa)$;
  end
end
return **D**;

Algorithm 1: Pseudocode of DO Algorithm

detection process for the received composite signal **r**. In MUD, detection order is one of the important factors which makes significant impact on the efficiency of the detector. The improvement due to DO is to be investigated in section 4.4.

4.4 Performance Evaluations

A series of computer simulations was conducted to verify the effectiveness of the proposed joint turbo equalization and BICM-ID-based IDMA system as well as to evaluate the impact of DO in frequency selective fading channels. As described above, first of all, all the parameters and labeling pattern are optimized by EBSA in AWGN channels; then, the optimal parameters and labeling pattern are applied into the proposed joint turbo equalization and BICM-ID-based IDMA system. It is shown that the proposed system with the optimal parameters determined by EBSA can achieve excellent performance in frequency selective fading channels.

4.4.1 EXIT Chart

The EXIT chart is presented in Fig. 4.3 to show the excellent matching between the demapper and decoder, where the SPC-IrR code parameters d_c, d_v, a, DACC doping ratio P, modulation mixing ratio D, and modulation labeling pattern obtained by using EBSA for 8 users, with SNR of each user $SNR_k = 0$ dB, are also provided in the figure. Such close matching between the demapper and decoder EXIT curves indicates that near-capacity performance can be expected in AWGN channels. Meanwhile, it also can be observed

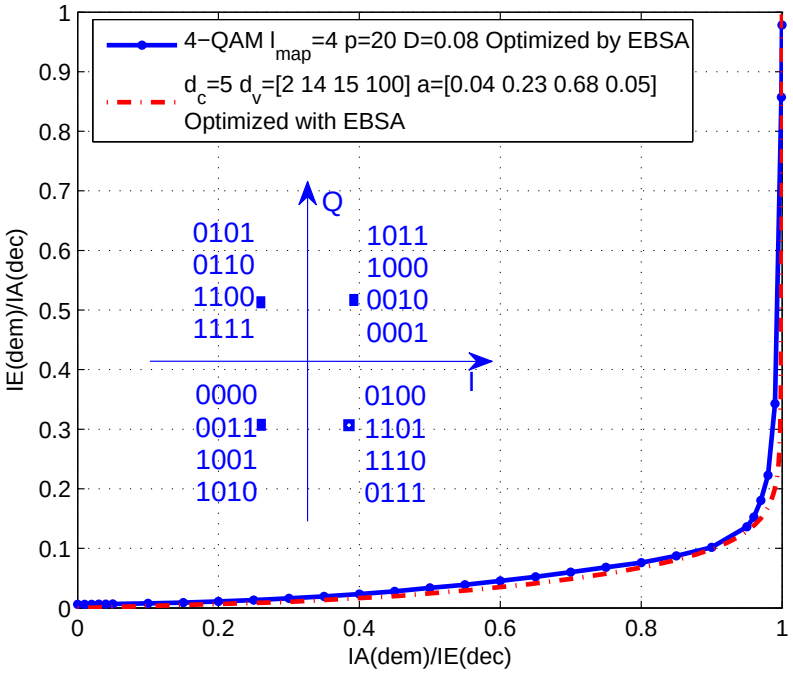

Figure 4.3: EXIT Chart for 8 users with $SNR_k = 0$ dB.

that the two EXIT curves reach a point very close to (1.0, 1.0) mutual information point so that the error floor in BER performance can be eliminated. The BER performances with EBSA in the case of single user SUD and MUD in AWGN channel are shown in **Chapter 3**. The effectiveness of utilizing the optimal codes parameters and labeling pattern designed for 8 users with $SNR_k = 0$ dB over frequency selective fading channels is to be investigated in subseciton 4.4.2.

4.4.2 FER Performances

This subsection presents the results of computer simulations conducted to evaluate the performance of the proposed system over frequency selective fading channels with the parameters of the transmission chain and labeling pattern obtained by EBSA. All simulations assumed that the channel frequency selectivity is due to an L-path propagation scenario with each path experiencing the block fading; L-path components have identical average power and independent complex Gaussian distribution.

In Fig. 4.4, it is shown that the FER performances of the proposed technique in the cases of single user, 8 users and 10 users with DO as well as the outage probability of the single user, where in all the cases with $L = 6$. The outage P_{out} is defined as

$$P_{out} = Pr(R > C), \tag{4.23}$$

which was evaluated via Monte Carlo simulations: C is the capacity of each channel realization, and the data was generated from 10,000,000 channel realizations. $R = 0.1394$ bits/s/Hz is the total per-Hz per-user transmission rate. Every outer iteration is followed by one round of inner iteration, expressed as (uO, vI), which represents that in total u outer iterations are performed, and each outer iteration is followed by v inner iterations (totaling $u \times v$ inner iterations).

It is found from Fig. 4.4 that the FER of single user with iterations (10O, 20I) shown with "$\circ$" has a very close performance to the single user outage probability bound shown by the dashed curve; only roughly 1 dB gap between them. Furthermore, the average FER[1] performances of 8 users and 10 users with iterations (10O, 20I), shown with "$\diamond$" and "$\square$", are not degraded too much compared to the single user's FER performance; there are only roughly 0.2 dB difference and 0.4 dB difference, respectively, when average SNR $\geqslant -3$ dB.

With a per-user rate of 0.1394, the system is equivalent to CDMA with spreading

[1]It is averaged over number of channel realization $\times$ number of users

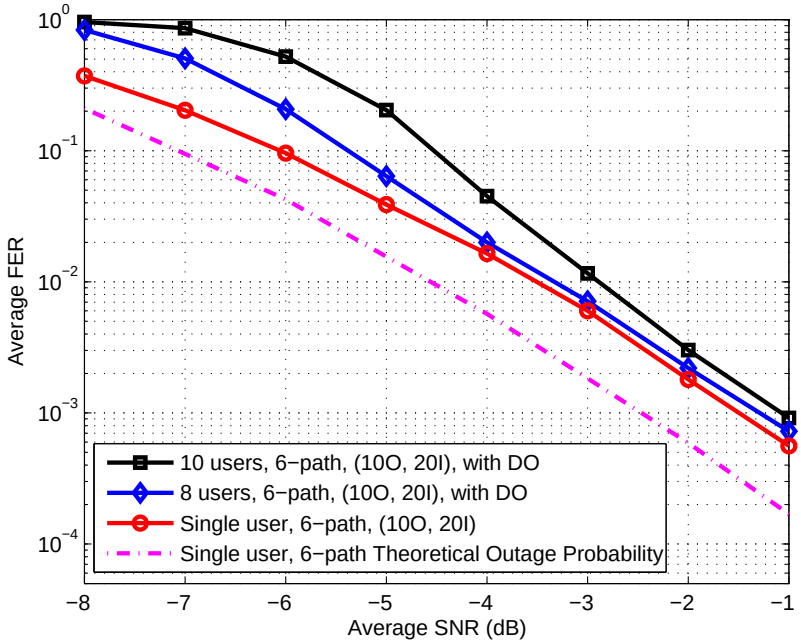

Figure 4.4: FER performance of the proposed system with single user, 8 users and 10 users.

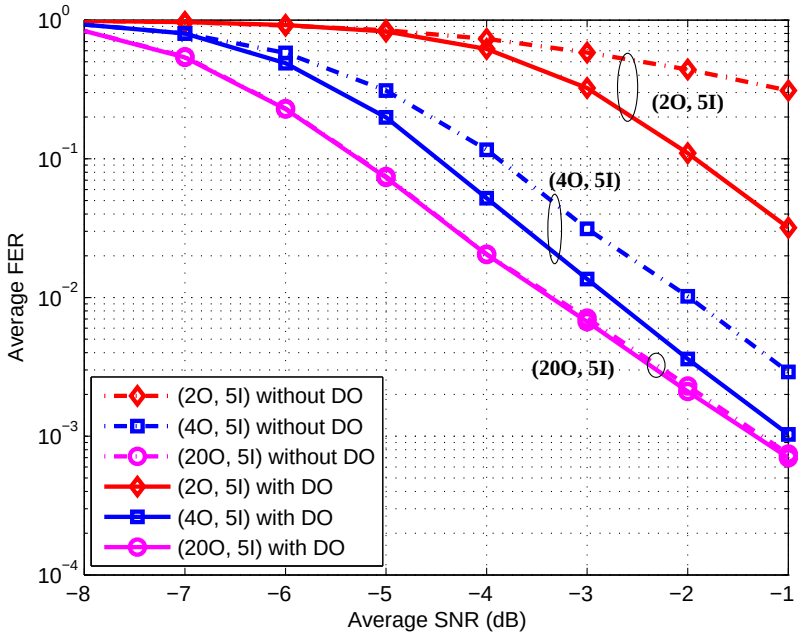

Figure 4.5: FER performance of the proposed system with and without DO, 8 users.

factor of 7.1736 $\approx$ 8 users. However, our results show that the proposed system still work well with 10 simultaneous users. The degradation is negligible compared with FER performance of 8 users, even though in this case, the equivalent spreading factor is larger than 8. It indicates that the non-linear soft-cancelation is out iteration combined with MMSE outperforms only linear MMSE signal detection at the SNR value larger than -3 dB.

Fig. 4.5 provides the average FER performance of the proposed system with and without DO, where $L = 6$ and $K = 8$, with several (u, v) pairs as a parameter. The solid curves in Fig. 4.5 present the average FER performance with DO, while the dashed curves without DO. It is clearly found from the figure that the system with DO outperform that without DO. This is because when numbers of the inner and outer iterations are not sufficient, such as (2O, 5I) and (4O, 5I), the interference from the other users can not be fully eliminated, as shown in the FER curves with "$\diamond$" and "$\square$", respectively. The reason is that the detection order of users in soft interference cancelation makes significant impact on the efficiency of the detector. With DO, the interference from the other users can be further eliminated with the same iteration times. However, from the average FER curves shown with "$\circ$", it can be found that the performances with the both cases become almost the same, because numbers of the inner and outer iterations are becoming large, as represented by (20O, 5I) in the figure. This is because, in the proposed system without DO, the interference from the other users can be also fully eliminated when sufficient inner and outer iterations are performed. It indicates that the proposed system requires more iteration times when no DO is used. However, (20O, 5I) is sufficient even without DO. It can therefore be concluded that the proposed system performance can further be enhanced with DO over without DO, if the tested iteration number is limited.

4.5 Summary

In this chapter, we have proposed a joint FD-SC-MMSE turbo equalization and IDMA signal detection technique for BICM-ID-based IDMA which works at a very low SNR range over frequency selective fading channels.

First of all, the proposed system model was introduced, and then followed by the detailed explanation of the scheme of joint turbo equalization and IDMA signal detection as well as the DO technique. The achievability of the close FER performance of single user with 6 paths corresponding to the outage probability was demonstrated by the simulations. It has been shown that the less degradation on FER performance for 10 users, with which

the user number exceeds the equivalent spreading factor 8.

Moreover, the comparison on the FER performances of the system with and without DO technique was made by the simulations. The results have shown significant performance improvement with DO technique, especially when the number of iteration is limited.

Chapter 5

Conclusions and Future Work

5.1 Conclusions

In this thesis, we have investigated an up-link multiple access technique with IDMA that requires proper operability at very low SINR range. The main contributions of this research are IDMA system designs based on BICM-ID scheme and EBSA optimization, which can achieve excellent near-capacity BER peformances in AWGN channels. Further jointly utilizing FD-SC-MMSE turbo equalization in frequency selective fading channels achieves the close FER performances to the outage probability. In particular, the impact of the power allocation on the convergence and the MAC rate region, the frame-asynchronism simulated by adding certain transmission delay, the effect of the DO technique, which can further improve the performance of the system or verify the properties of the system, were also provided.

In **Chapter 3**, we focused on IDMA system design and its properties that requires proper operability at very low SINR range. First of all, we verified that the near-capacity performance of BICM-ID using very low rate SPC-IrR codes, designed by EBSA, is also effective when it is applied into the proposed BICM-ID-based IDMA system. It has been shown that near-capacity performance, very sharp BER threshold and error floor removal (or at least reduced to a value range below $10^{-6} - 10^{-5}$ of BER) can be achieved at a very low SINR range where IDMA systems are required to properly work. Motivated by the very sharp BER threshold, a new yet simple MUD technique for IDMA was proposed, which does not require heavy per-iteration computational burden. The research then analyzed the convergence and the MAC rate region properties. Multi-dimensional EXIT chart was used as a tool for the analyses. It has been shown that even though the demapper and decoder's EXIT planes are very closely matched, the trajectory sneaks

through the small gap between the planes and reaches a point very close to the (1.0, 1.0, 1.0) mutual information point. After that, results of the MAC rate region analysis show that to achieve the same spectrum efficiency, unequal power allocation requires smaller MAC rate region (or MAC-pentagon) compared with the equal power allocation; the proposed IDMA technique outperforms a counterpart technique in terms of the rate pair relative to the MAC region. The results of the performance analyses and evaluations shown in this thesis were all consistent with each other. Furthermore, a CHADE technique was proposed to investigate frame-asynchronism with the proposed IDMA system by adding certain transmission delay for each user. Simulation results indicated that the proposed IDMA technique is robust to against frame-asynchronism.

In **Chapter 4**, we proposed a joint turbo equalization and IDMA signal detection as well as DO technique for the proposed IDMA at very low SNR range in frequency selective fading channels. The EBSA technique were also applied to optimize the codes parameters and labeling patterns. The achieved performances of the proposed system demonstrated by the computer simulations were threefold: (1) close FER performance of single user with 6 paths to the outage probability; (2) less degradation on FER performance for 10 users even with the equivalent spreading factor of 8 (code rate $R = 0.1394$ bits/s/Hz); (3) significant performance improvement with DO technique compared with that of without DO technique, especially when the number of iteration is limited, due to, e.g., power constraint at the base stations. As a whole, the proposed joint turbo equalization and BICM-ID-based IDMA technique is suitable for future multiple access wireless communication systems, especially for reliable transmission at very low SNR range.

5.2 Future Work

Based on the achievements of this research and in order to best utilize the obtained results, applying the proposed IDMA techniques into the cooperative communications is a very interesting topic being as future work.

Nowadays, the speed of the development of wireless communications has been becoming very rapidly. Current communications standards and systems are not optimally prepared for applied in unpredictable environments such as serious disaster scenarios such as earthquakes or tsunamis. Cellular communications systems are planned using accurate link budget allocation mechanisms, in order to keep the outage probability in an acceptable level. However, future networks will most likely be heterogeneous and dense, a structure which can be exploited if communication schemes are constructed on an appropriate the

theoretical, technological, and practical basis. In order to build such fundamental bases, EU FP7 RESCUE[1] project proposes integrated concept links-on-the fly to cope with the wireless communications in unpredictable environments, which involve: (a). Asynchronous transmission; (b). Many unreliable (lossy) links.

Since the future work of this research is along with EU FP7 RESCUE project, which JAIST is an official member of, the aim of this future work is to best exploit the superiority of joint utilization of BICM-ID-based IDMA and cooperative communications to propose the new communication technique which is suitable for unpredictable environment. The future work would be focusing on: (1) utilizing BICM-ID-based IDMA as one of suitable access techniques for asynchronous transmission to manage problem (a), since BICM-ID-based IDMA is very robust against asynchronism; (2) utilizing cooperative communication with best exploitation of the source correlation to improve the system performance so as to deal with problem (b), since cooperative communications can improve the performance of system with unreliable (lossy) links. By best utilizing the proposed IDMA technique into cooperative communication system, a robust and efficient communication system can be proposed to fulfill unpredictable situations which are frequent in todays wireless networks with mobility of nodes, high density cells, dynamic and opportunistic frequency management.

The purpose of the future work is to best exploit the joint utilization of IDMA and cooperative communications. It is well known that IDMA is an access technique for MAC, and Slepian-Wolf theorem is one of the most representative theorem for cooperative communications. Hence, in other words, the goal of this future work is to best exploit the MAC and Slepian-Wolf properties in wireless cooperative communications.

The most difficult part of the future work is to exploit the intersection of IDMA's MAC rate region and cooperative communications Slepian-Wolf rate region, which indicates that applying IDMA into cooperative communications to allow the signals from different users to be transmitted simultaneously. The challenges are divided into two parts: (1) to best exploit the superiority of the MAC channel over the orthogonal signaling; (2) to best exploit the source correlation knowledge in MUD scenario.

The expected impact of this future work is significant: with both of the superior properties of MAC and Slepian-Wolf coding, the technique is expected to achieve an excellent performance against frame-asynchronous transmission and unreliable (lossy) links, which are initialed in the unpredictable environments.

[1]RESCUE Project full title: links-on-the-fly technology for Robust, Efficient and Smart Communication in Unpredictable Environments. Grant agreement no: 619555

Appendix A

Gaussian Noise Approximation

As stated in [32], it is well-known that when the number of users increases, in multiple access system, the interference from the other users can be approximated as Gaussian noise according to the central limit theorem. However, it is assumed that instantaneous power control and furthermore the phase rotations have been ignored, which is eventually equivalent to the scenario where all the users transmit the same static AWGN channel. To identify the impact of this assumption on the demapper's *extrinsic* mutual information, we evaluate the EXIT curve for $K = 2$, which is the worst scenario, where each user has randomly different phase rotation, resulting in more Gaussian-like receive signal point distribution. The received signal in this case can be expressed as

$$r_m = \sqrt{P_k} \cdot x_{k,m} \cdot e^{j\theta_k} + \zeta_{k,m}, \tag{A.1}$$

where θ_k denotes the phase rotation of k-th user, uniformly distributed over $[0, 2\pi]$. The comparison between the two cases is presented in Fig. A.1 in terms of the demapper's EXIT curves. It can be observed that the difference in the EXIT curves is negligible.

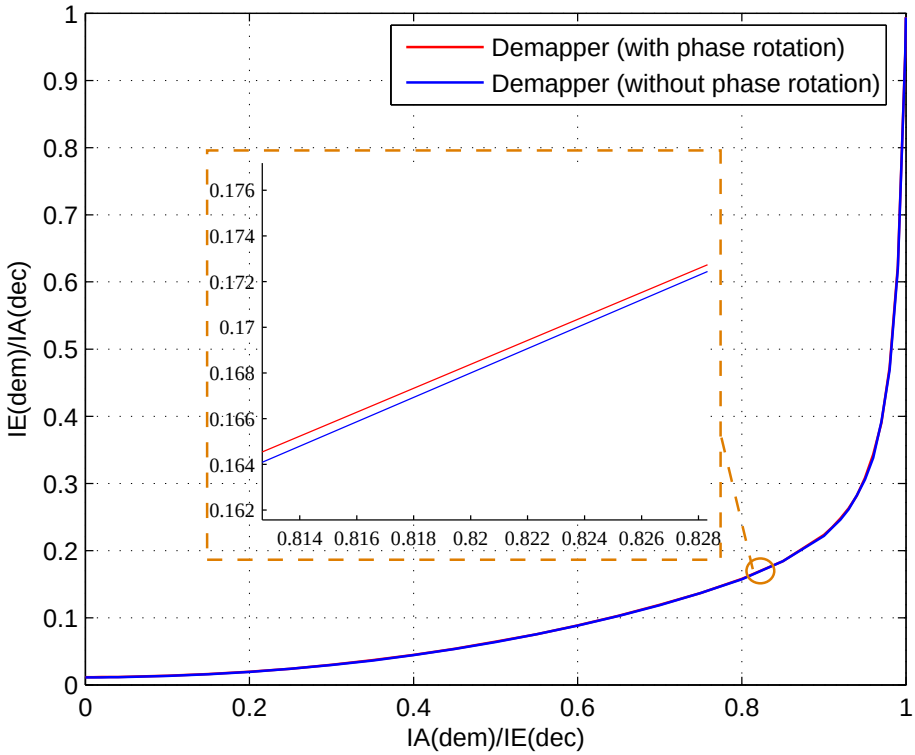

Figure A.1: Comparison between the EXIT curves of demapper for transmitted signals with and without phase rotation, $K = 2$ users, $SNR = -3.8$ dB.

Abbreviations and Notations

AWGN	additive white Gaussian noise
BCJR	MAP algorithm proposed by Bahl, Cocke, Jelinek, Raviv
BER	bit error rate
BICM-ID	bit-interleaved coded modulation with iterative detection
BSA	binary switching algorithm
CDMA	code division multiple access
cdf	cumulative density function
CHADE	chained detection
CP	cyclic prefix
DACC	doped accumulator
DACC^{-1}	doped accumulator decoder
DO	detection ordering
EBSA	EXIT-constrained binary switching algorithm
EM	extended mapping
ESE	elementary signal estimator
EXIT	extrinsic information transfer
EM^{-1}	extended mapping demapping
FD-SC-MMSE	frequency domain soft-interference concelation minimum mean-square error
FDMA	frequency division multiple access
FER	frame error rate
IDMA	interleaver division multiple access
IrR	irregular repetition code
ISI	inter-symbol interference
LDPC	low density parity check
LLR	log-likelihood ratio
LP	linear programming
MAI	multiple access interference
MAC	multiple access channel
MUD	multiuser detection
pdf	probability density function
QAM	quadrature amplitude modulation
RA	Repeat Accumulate

SINR	signal-to-interference-plus-noise power ratio
SNR	signal-to-noise power ratio
SPC	single parity check code
SSIC	soft successive interference cancellation
SUD	single user detection
TDMA	time division multiple access
TCM	Trellis-coded-modulation
2D	two-dimensional
3D	three-dimensional

$\hat{(\cdot)}$	estimation of the argument
$(\cdot)^{-1}$	inverse of the argument
$\exp(\cdot)$	exponential calculation of the argument
$E[\cdot]$	expectation of a random variable
$\log_2(\cdot)$	natural logarithm to base 2
$\log(\cdot)$	natural logarithm to any bases
$\max(\cdot)$	maximum value
$\min(\cdot)$	minimum value
$H(\cdot)$	entropy
$H(\cdot\|\cdot)$	conditional entropy
$H(\cdot,\cdot)$	joint entropy
$I(\cdot,\cdot)$	mutual information between argument 1 and 2

K	simultaneous user number
$b_{k,i}$	information bit of user k at timing index i
$\mathbf{b}_k$	information bit sequence of user k
$u_{k,j}$	accumulated coded bit of user k at timing index j
$\mathbf{u}_k$	accumulated coded bit sequence of user k
$x_{k,m}$	transmitted bit of user k at timing index m
$\mathbf{x}_k$	transmitted bit sequence of user k
r_m	received signal at timing index m
$\mathbf{r}$	received signal sequence

$\hat{b}_{k,i}$	estimated information bit sequence of user k at timing index i
$\hat{\mathbf{b}}_k$	estimated information bit sequence of user k
$L_{k,a,dem,j}$	*a priori* demapper's LLR of user k at timing index j
$\mathbf{L}_{k,a,dem}$	*a priori* demapper's LLR sequence of user k
$L_{k,e,dem,j}$	*extrinsic* demapper's LLR of user k at timing index j
$\mathbf{L}_{k,e,dem}$	*extrinsic* demapper's LLR sequence of user k
$L_{k,a,dec,j}$	*a priori* SPC-IrR decoder's LLR of user k at timing index j
$\mathbf{L}_{k,a,dec}$	*a priori* SPC-IrR decoder's LLR sequence of user k
$L_{k,e,dec,j}$	*extrinsic* SPC-IrR decoder's LLR of user k at timing index j
$\mathbf{L}_{k,e,dec}$	*extrinsic* SPC-IrR decoder's LLR sequence of user k
$L_{k,p,dacc,j}$	*a posteriori* doped accumulator decoder's LLR of user k at timing index j
$\mathbf{L}_{k,p,dacc}$	*a posteriori* doped accumulator decoder's LLR sequence of user k
$\hat{L}_{k,p}$	*a posteriori* LLR sequence fed back to soft-symbol generator
$IA(dem)$	*a priori* information for demapper and doped accumulator
$IE(dem)$	*extrinsic* information for demapper and doped accumulator
$IA(dec)$	*a priori* information for decoder
$IE(dec)$	*extrinsic* information for decoder
$\lvert \cdot \rvert$	absolute value
Π	interleaver
Π^{-1}	de-interleaver
σ_n^2	Gaussian noise variance
N_0	the two-sided spectral density of the noise

Bibliography

[1] C. Berrou, A. Glavieux, and P. Thitimajshima, "Near Shannon limit error-correction coding and decoding: Turbo code," in *IEEE ICC'93*, (Geneva), pp. 1064–1070, May 1993.

[2] A. J. Viterbi, "Very low rate convolutional codes for maximum theoretical performance of spread spectrum multiple-access channels," *IEEE J. Select. Areas Commun.*, vol. 8, pp. 641–649, August 1990.

[3] S. Verdu and S. Shamai, "Spectral efficiency of cdma with random spreading," *IEEE Transactions on Information Theory*, vol. 45, pp. 622–640, March 1999.

[4] A. J. Viterbi, "Spread spectrum communications-myths and realities," *IEEE Communications Magazines.*, vol. 23, May 1979.

[5] P. Frenger, P. Orten, and T. Ottosson, "Code-spread CDMA using maximum free distance low-rate convolutional codes," *IEEE Transactions on Communications*, vol. 48, pp. 135–144, January 2000.

[6] H. Schoeneich and P. A. Hoeher, "Adaptive interleave-division multiple access – a potential air interference for 4G bearer services and wireless LANs," in *WOCN*, (Muscat, Oman), pp. 179–182, June 2004.

[7] P. A. Hoeher and H. Schoeneich, "Interleave-division multiple access from a multiuser point of view," in *5-th Int. Symp. Turbo Codes Related Topics Connection 6th Int. ITG-Conf. Source Channel Coding*, (Germany), pp. 140–144, April 2006.

[8] P. Li, L. Liu, K. Wu, and W. K. Leung, "Interleave division multiple access," *IEEE Transactions on Wireless Communications*, vol. 5, pp. 938–947, April 2006.

[9] K. Kusume, G. Bauch, and W. Utschick, "IDMA vs. CDMA: detectors, performance

and complexity," in *IEEE Global Telecommunications Conference (GLOBECOM 2009)*, (Hawaii, USA), pp. 1–8, November 2009.

[10] H. H. Chung, Y. C. Tsai, and M. C. Lin, "IDMA using non-Gray labelled modulation," *IEEE Transactions on Communications*, vol. 59, pp. 2492–2501, September 2011.

[11] K. Fukawa, S. Ormsub, A. Tolli, K. Anwar, and T. Matsumoto, "EXIT-constrained BICM-ID design using extended mapping," *EURASIP Journal on Wireless Commun. and Networking*, vol. 2012, February 2012.

[12] C. E. Shannon, "A mathematical theory of communications," *Bell Systems Technical Journal*, vol. 27, pp. 379–423,623–656, 1948.

[13] G. L. Stuber, *Principles of Mobile Communications*. Norwell, MA: Kluwer, 1996.

[14] S. ten Brink, "Convergence of iterative decoding," *Electronics Letters*, vol. 35, pp. 806 –808, May 1999.

[15] S. ten Brink, "Convergence behavior of iteratively decoded parallel concatenated codes," *IEEE Transactions on Communications*, vol. 49, pp. 1727–1737, October 2001.

[16] T. M. Cover and J. A. Thomas, *Elements of Information theory 2nd Edition*. USA: John Wiley & Sons, Inc.,, 2006.

[17] S. ten Brink, "Code characteristic matching for iterative decoding of serially concatenated codes," *Annals of Telecommunications*, vol. 56, pp. 394–408, 2001.

[18] F. Brannstrom, L. Rasmussen, and A. Grant, "Convergence analysis and optimal scheduling for multiple concatenated codes," *IEEE Transactions on Information Theory*, vol. 51, pp. 3354–3364, September 2005.

[19] E. Zehavi, "8-psk trellis codes for a rayleigh channel," *IEEE Transactions on Communications*, vol. 40, no. 5, pp. 873–884, 1992.

[20] L. Hanzo, T. Liew, and B. Yeapi, *Turbo Coding, Turbo Equalisation and Space-Time Coding: For Transmission over Fading Channels*. John Wiley & Sons, West Sussex, 2002.

[21] X. Li and J. Ritcey, "Bit-interleaved coded modulation with iterative decoding," *Communications Letters, IEEE*, vol. 1, no. 6, pp. 169–171, 1997.

[22] X. Li and J. Ritcey, "Trellis-coded modulation with bit interleaving and iterative decoding," *IEEE Journal on Selected Areas in Communications*, vol. 17, no. 4, pp. 715–724, 1999.

[23] D. Zhao, A. Dauch, and T. Matsumoto, "BICM-ID using extended mapping and repetition code with irregular node degree allocation," in *Vehicular Technology Conference (VTC) Spring*, (Barcelona), pp. 1–5, April 2009.

[24] K. Fukawa, D. Zhao, A. Tlli, and T. Matsumoto, "Irregular repetition and single parity check coded BICM-ID using extended mapping -optimal node degree allocation," in *2010 5th International ICST Conf. on Commun. and Networking in China (CHINACOM)*, (Beijing), pp. 1–6, August 2010.

[25] P. Henkel, "Extended mappings for bit-interleaved coded modualtion," in *IEEE International Symposium on Personal, Indoor, and Mobile Radio Communications (PIMRC)*, (Helsinki), pp. 1–4, September 2006.

[26] F. S. S. Pfletschinger, "Error floor removal for bit-interleaved coded modulation with iterative detection," *IEEE Transactions on Wireless Communications*, vol. 5, no. 11, pp. 3174–3181, 1992.

[27] K. Anwar and T. Matsumoto, "Very simple BICM-ID using repetition code and extended mapping with doped accumulator," *Wireless Personal Communications, Springer*, September 2011. doi:10.1007/s11277-011-0397-1.

[28] J. Hagenauer, "The EXIT chart - Introduction to extrinsic information transfer in iterative processing," in *12th European Signal Processing Conference (EUSIPCO)*, (Vienna, Austria), pp. 1541–1548, September 2004.

[29] J. H. G. B. F. Schreckenbach, N. Gortz, "Optimal symbol mappings for bit-interleaved coded modulation with iterative decoding," in *Global Telecommunication Conference (GLOBECOM'03)*, (San Francisco), p. 6, December 2003.

[30] F. Schreckenbach and G. Bauch, "Irregular signal constellations, mappings and precoder," in *Information Theory and its Applications (ISITA)*, (Italy), pp. 10–13, October 2004.

[31] P. Wang, J. Xiao, and P. Li, "Comparison of orthogonal and non-orthogonal approaches to future wireless cellular systems," *IEEE Vehicular Technology Magazine*, vol. 1, September. 2006.

[32] K. Wu, K. Anwar, and T. Matsumoto, "BICM-ID-based IDMA: Convergence and rate region analyses," *IEICE transactions on communications*, vol. E97-B, pp. 1483–1492, July 2014.

[33] R. Lidl and H. Niederreiter, *Finite Fields*. Cambridge University Press, 1996.

[34] S. Lin and D. J. Costello, *Error Control Coding*. Prentice Hall, Inc., NJ, USA., 2nd ed., 2004.

[35] S. Verdu, *Multiuser Detection*. Cambridge University Press, 1998.

[36] K. Wu, K. Anwar, and T. Matsumoto, "Joint turbo equalization and BICM-ID-based IDMA over frequency selective fading channels," in *International Symposium on Information Theory and Its Applications (ISITA)*, (Melbourne, Australia), October 2014, accepted.

[37] K. Kansanen and T. Matsumoto, "An analytical method for MMSE MIMO turbo equalizer EXIT chart computation," *IEEE Transactions on Wireless Communication*, vol. 6, January 2007.

Achievements

Journal Article

- K. Wu, K. Anwar, T. Matsumoto, BICM-ID-based IDMA: Convergence and rate region analyses, IEICE transactions on communications, vol. E97-B, no. 7, pp. 1483-1492, July 2014.

Conference Articles

- K. Wu, K. Anwar, T. Matsumoto, BICM-ID-based IDMA over Multipath Fading Channels, IEICE General Conference 2014, Niigata, March 18-21, 2014.
- K. Wu, K. Anwar, T. Matsumoto, Joint turbo equalization and BICM-ID-based IDMA over frequency selective fading channels, International Symposium on Information Theory and Its Applications (ISITA) 2014, Melbourne, Australia, October 26-29. (Accepted)

European COST Action IC 1004

- K. Wu, K. Anwar, T. Matsumoto, Joint Turbo Equalization and BICM-ID-based IDMA over Frequency Selective Fading Channels, the Temporary Document (TD) accepted by and presented in EU (COST) 9th IC1004 MC Meeting, February 2014, Ferrara, Italy.

Presentations in Academic Visits

- K. Wu, K. Anwar, T. Matsumoto, BICM-ID-based IDMA using Extended Mapping, presented in City University of Hong Kong, March, 2013, Hong Kong.
- K. Wu, K. Anwar, T. Matsumoto, BICM-ID-based IDMA over Frequency Selective Fading Channels, presented in City University of Hong Kong, November, 2013, Hong Kong.